

# c-MAF-dependent regulatory T cells mediate immunological tolerance to a gut pathobiont

Mo Xu<sup>1\*</sup>, Maria Pokrovskii<sup>1\*</sup>, Yi Ding<sup>2</sup>, Ren Yi<sup>3</sup>, Christy Au<sup>1,4</sup>, Oliver J. Harrison<sup>5</sup>, Carolina Galan<sup>1</sup>, Yasmine Belkaid<sup>5,6</sup>, Richard Bonneau<sup>3,7,8</sup> & Dan R. Littman<sup>1,4</sup>

**Both microbial and host genetic factors contribute to the pathogenesis of autoimmune diseases<sup>1–4</sup>.** There is accumulating evidence that microbial species that potentiate chronic inflammation, as in inflammatory bowel disease, often also colonize healthy individuals. These microorganisms, including the *Helicobacter* species, can induce pathogenic T cells and are collectively referred to as pathobionts<sup>4–6</sup>. However, how such T cells are constrained in healthy individuals is not yet understood. Here we report that host tolerance to a potentially pathogenic bacterium, *Helicobacter hepaticus*, is mediated by the induction of ROR $\gamma$ T<sup>+</sup>FOXP3<sup>+</sup> regulatory T (iT<sub>reg</sub>) cells that selectively restrain pro-inflammatory T helper 17 (T<sub>H</sub>17) cells and whose function is dependent on the transcription factor c-MAF. Whereas colonization of wild-type mice by *H. hepaticus* promoted differentiation of ROR $\gamma$ T-expressing microorganism-specific iT<sub>reg</sub> cells in the large intestine, in disease-susceptible IL-10-deficient mice, there was instead expansion of colitogenic T<sub>H</sub>17 cells. Inactivation of c-MAF in the T<sub>reg</sub> cell compartment impaired differentiation and function, including IL-10 production, of bacteria-specific iT<sub>reg</sub> cells, and resulted in the accumulation of *H. hepaticus*-specific inflammatory T<sub>H</sub>17 cells and spontaneous colitis. By contrast, ROR $\gamma$ T inactivation in T<sub>reg</sub> cells had only a minor effect on the bacteria-specific T<sub>reg</sub> and T<sub>H</sub>17 cell balance, and did not result in inflammation. Our results suggest that pathobiont-dependent inflammatory bowel disease is driven by microbiota-reactive T cells that have escaped this c-MAF-dependent mechanism of iT<sub>reg</sub>-T<sub>H</sub>17 homeostasis.

We chose *H. hepaticus* as a model to investigate host-pathobiont interactions. Blockade of IL-10RA induced inflammation of the large intestine in *H. hepaticus*-colonized *Il23r<sup>GFP</sup>* reporter mice<sup>5,6</sup>, increasing the proportion of green fluorescent protein-positive (GFP<sup>+</sup>) cells (predominantly T<sub>H</sub>17 cells) from approximately 10% to 50% of large intestine CD4<sup>+</sup> T cells (Extended Data Fig. 1a). We therefore sought to determine why *H. hepaticus*-induced T cells do not cause disease in wild-type mice at the steady state. To address this question, we first identified the T cell receptor (TCR) sequences and cognate epitopes of *H. hepaticus*-induced T<sub>H</sub>17 cells that expand during inflammation, and subsequently traced the fate of these cells at the steady state.

We cloned individual TCR sequences from colitogenic IL-23R-GFP<sup>+</sup> T cells (Extended Data Fig. 1b) and found that nine out of twelve clonotypic TCRs were *H. hepaticus*-specific (Extended Data Fig. 1c). We subsequently identified<sup>7,8</sup> a *H. hepaticus*-unique protein, HH\_1713, that contains two immunodominant epitopes. The E1 peptide epitope, presented by I-A<sup>b</sup>, was recognized by *H. hepaticus*-specific TCR HH5-1, whereas E2 was recognized by TCR HH5-5, HH6-1 and HH7-2 (Extended Data Fig. 1c). We next developed two complementary

approaches to track *H. hepaticus*-specific T cells *in vivo*<sup>9,10</sup>, HH7-2 and HH5-1 TCR transgenic mice (HH7-2tg and HH5-1tg) and a major histocompatibility complex (MHC) class II tetramer loaded with E2 peptide (HH-E2 tetramer) (Extended Data Fig. 1d–g).

To track what happens to *H. hepaticus*-specific T cells in healthy mice, we simultaneously transferred naive T cells from HH7-2tg and 7B8tg (segmented filamentous bacteria (SFB)-specific TCRtg control)<sup>8</sup> mice into wild-type mice that were stably colonized with *H. hepaticus* and SFB (Fig. 1a). Two weeks after adoptive transfer, HH7-2tg donor cells were enriched in the large intestinal lamina propria (LILP) and caecal patch, whereas 7B8tg cells predominated in the small intestinal lamina propria (SILP) and Peyer's patches (Extended Data Fig. 2a, b), consistent with colonization of *H. hepaticus* in the large intestine and SFB in the small intestine. As previously reported, 7B8 cells developed into T<sub>H</sub>17 cells that were largely positive for ROR $\gamma$ T and negative for FOXP3<sup>8</sup> (Fig. 1b, c, Extended Data Fig. 2c, d). By contrast, HH7-2tg cells in the LILP were mostly iT<sub>reg</sub> cells that express both ROR $\gamma$ T and FOXP3 (approximately 60% of total donor-derived HH7-2tg cells)<sup>11,12</sup>, rather than T<sub>H</sub>17 cells (less than 10% of total HH7-2tg cells) (Fig. 1b, c, Extended Data Fig. 2c, d). Notably, two other colonic T<sub>reg</sub> cell markers, GATA3 and ST2, were not expressed on HH7-2tg cells<sup>13</sup> (Extended Data Fig. 2e). 7B8tg and HH7-2tg T cells that expressed neither ROR $\gamma$ T nor FOXP3 were mostly T follicular helper (T<sub>FH</sub>) cells and were enriched in the Peyer's patches and caecal patch (Fig. 1b, c, Extended Data Fig. 2c, d). Breeding HH7-2tg mice onto the *Rag1*<sup>−/−</sup> background excluded the possibility that HH7-2tg iT<sub>reg</sub> cells detected after adoptive transfer were contaminated by thymus-derived natural T<sub>reg</sub> (nT<sub>reg</sub>) cells or were influenced by the presence of dual TCRs (Extended Data Fig. 3a–c). Adoptively transferred HH5-1tg and HH-E2-tetramer-positive cells had differentiation profiles similar to HH7-2tg cells (Fig. 1d, e, Extended Data Figs 2f and 3d, e). These results indicate that the host responds to *H. hepaticus* by generating immunotolerant iT<sub>reg</sub> cells rather than pro-inflammatory T<sub>H</sub>17 cells.

To examine whether the iT<sub>reg</sub> cell-dominant differentiation of *H. hepaticus*-specific T cells is altered during intestinal inflammation, we co-transferred naive HH7-2tg and control 7B8tg T cells into colonized *Il10*<sup>−/−</sup> recipients. Notably, only a small proportion of the transferred HH7-2tg T cells expressed FOXP3 in the LILP. Instead, most of them differentiated into pro-inflammatory T<sub>H</sub>17 cells with T<sub>H</sub>1-like features, characterized by the expression of both ROR $\gamma$ T and T-bet and high levels of IL-17A and IFN $\gamma$  upon re-stimulation<sup>14</sup> (Fig. 2a–f, Extended Data Fig. 4a, c, d). These results were recapitulated with HH5-1tg T cell adoptive transfer and endogenous HH-E2 tetramer<sup>+</sup> T cells (Extended Data Fig. 4e–g). By comparison, disruption of IL-10-mediated immune tolerance did not result in deviation of

<sup>1</sup>Molecular Pathogenesis Program, The Kimmel Center for Biology and Medicine of the Skirball Institute, New York University School of Medicine, New York, New York 10016, USA. <sup>2</sup>Department of Pathology and Laboratory Medicine, University of Rochester Medical Center, Rochester, New York 14642, USA. <sup>3</sup>Courant Institute of Mathematical Sciences, Computer Science Department, New York University, New York, New York 10003, USA. <sup>4</sup>The Howard Hughes Medical Institute, New York University School of Medicine, New York, New York 10016, USA. <sup>5</sup>Mucosal Immunology Section, Laboratory of Parasitic Diseases, National Institute of Allergy and Infectious Diseases, NIH, Bethesda, Maryland 20892, USA. <sup>6</sup>NIAID Microbiome Program, NIH, Bethesda, Maryland 20892, USA. <sup>7</sup>Center for Genomics and Systems Biology, Department of Biology, New York University, New York, New York 10003, USA. <sup>8</sup>Center for Computational Biology, Flatiron Institute, Simons Foundation, New York, New York 10010, USA.

\*These authors contributed equally to this work.

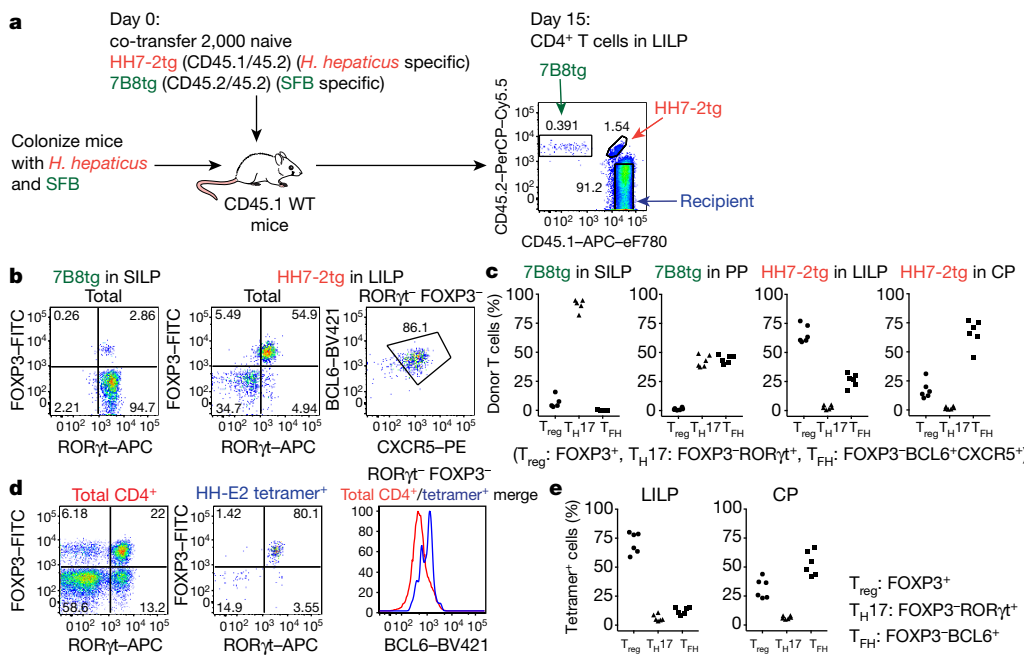
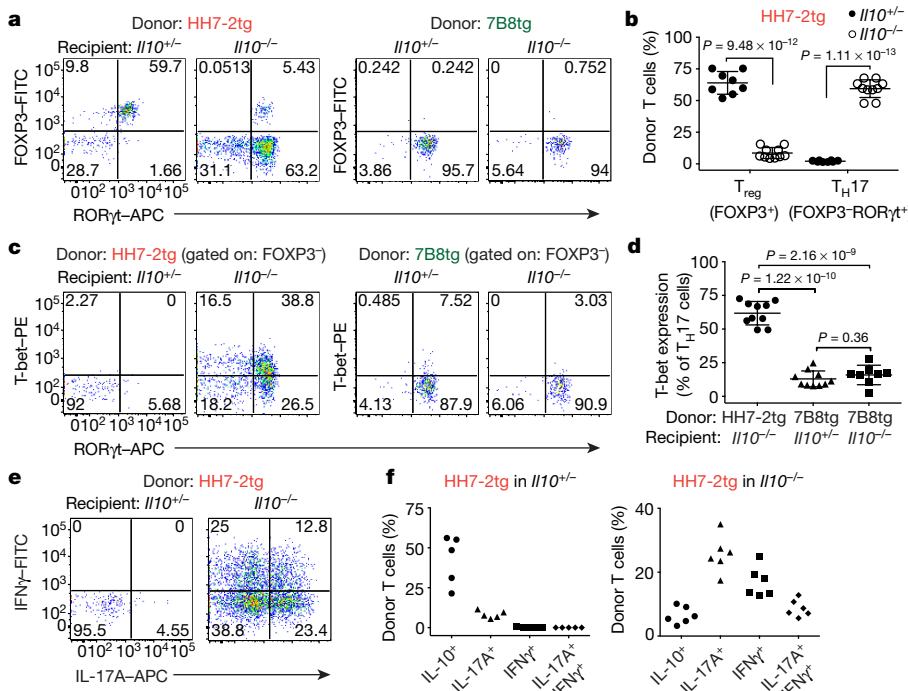


**Figure 1 | *H. hepaticus* induces ROR $\gamma$ t<sup>+</sup> T<sub>reg</sub> and T<sub>FH</sub> cell responses under steady state.** **a**, Experimental scheme for co-transfer of congenic isotype-labelled HH7-2tg and 7B8tg cells into wild-type (WT) mice colonized with *H. hepaticus* and SFB. **b, c**, ROR $\gamma$ t, FOXP3, BCL6 and CXCR5 expression (**b**) and frequencies of T<sub>reg</sub> (FOXP3<sup>+</sup>), T<sub>H</sub>17 (FOXP3<sup>-</sup>ROR $\gamma$ t<sup>+</sup>) and T<sub>FH</sub> (BCL6<sup>+</sup>CXCR5<sup>+</sup>) (**c**) among donor-derived T cells in indicated tissues. Data are from 1 of 3 experiments, with n = 15 in the 3 experiments. CP, caecal patch; PP, Peyer's patches. APC

SFB-specific T<sub>H</sub>17 cells to the inflammatory T<sub>H</sub>17-T<sub>H</sub>1 cell phenotype (Fig. 2c, d, Extended Data Fig. 4a–d). Furthermore, we observed similar deviated T cell responses to *H. hepaticus* in models of T cell transfer colitis and *Citrobacter rodentium*-induced colonic inflammation, but not in dextran sulfate sodium (DSS) colitis, an innate immunity-dependent model (Extended Data Fig. 5a–h). Commensal microorganism-specific T cells can thus acquire pro-inflammatory phenotypes



(allophycocyanin), Cy5.5, eF780, FITC, PE (phycoerythrin) and PerCP denote fluorochrome labels. **d, e**, Wild-type mice (n = 6) were colonized with *H. hepaticus* for 3–4 weeks and analysed for ROR $\gamma$ t, FOXP3 and BCL6 expression in total CD4<sup>+</sup> (red) and HH-E2 tetramer<sup>+</sup> (blue) T cells from the LILP (**d**) and frequencies of T<sub>reg</sub> (FOXP3<sup>+</sup>), T<sub>H</sub>17 (FOXP3<sup>-</sup>ROR $\gamma$ t<sup>+</sup>) and T<sub>FH</sub> (BCL6<sup>+</sup>) cells among HH-E2 tetramer<sup>+</sup> T cells in the LILP and caecal patch (**e**). Data summarize two independent experiments.

during enteric infection<sup>15</sup>, although the high frequency of such infections suggests the existence of a mechanism to re-establish gut tolerance. Our observations of *H. hepaticus*-specific iT<sub>reg</sub>-T<sub>H</sub>17 skewing during colitis are consistent with a contemporaneous study using two different *Helicobacter* species<sup>16</sup>. These findings indicate that dysregulated T cell tolerance to pathobionts may be a general hallmark of inflammatory bowel disease.

**Figure 2 | *H. hepaticus* predominantly induces inflammatory T<sub>H</sub>17 cells in IL-10 deficiency-dependent colitis.** **a–d**, LILP HH7-2tg and SILP 7B8tg donor-derived cells in II10<sup>+/−</sup> (n = 8) and II10<sup>−/−</sup> (n = 10) mice were analysed for FOXP3 and ROR $\gamma$ t expression (**a**), frequencies of T<sub>reg</sub> (FOXP3<sup>+</sup>) and T<sub>H</sub>17 (FOXP3<sup>-</sup>ROR $\gamma$ t<sup>+</sup>) cells (**b**), ROR $\gamma$ t and T-bet co-expression (**c**), and frequencies of T-bet expression among T<sub>H</sub>17 (FOXP3<sup>-</sup>ROR $\gamma$ t<sup>+</sup>) cells (**d**). Data are from four independent experiments. **e, f**, IL-17A and IFN $\gamma$  expression (**e**) and frequencies of IL-10<sup>+</sup>, IL-17A<sup>+</sup> and IFN $\gamma$ <sup>+</sup> cells (**f**) among LILP HH7-2tg donor-derived cells in II10<sup>+/−</sup> (n = 5) and II10<sup>−/−</sup> (n = 6) mice after re-stimulation. Data summarize two independent experiments. All statistics were calculated by unpaired two-sided Welch's t-test. Error bars denote mean ± s.d. P values are indicated on the figure.

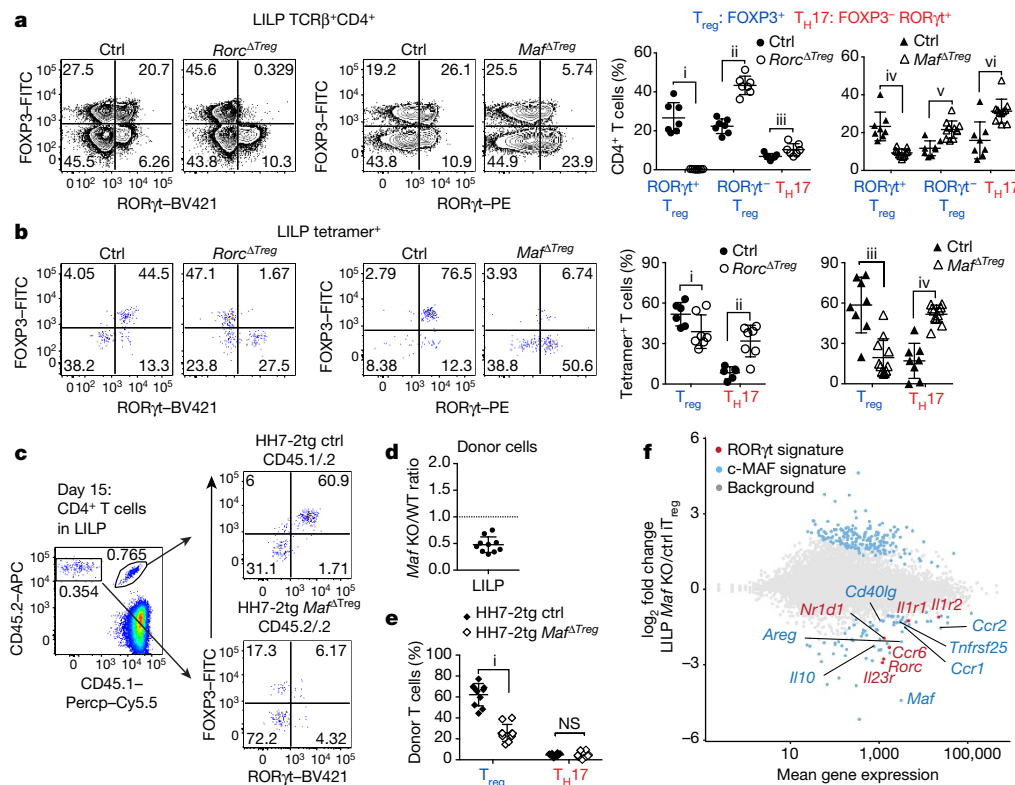


**Figure 3 | c-MAF is required for the differentiation and function of induced T<sub>reg</sub> cells in the gut.** **a, b,** Transcription factor staining in total CD4<sup>+</sup> (**a**) and HH-E2 tetramer<sup>+</sup> (**b**) T cells from the LILP of indicated mice. Left, ROR $\gamma$ t and FOXP3 expression. Right, frequencies of indicated T<sub>reg</sub> (FOXP3<sup>+</sup>) and TH17 (FOXP3<sup>-</sup>ROR $\gamma$ t<sup>+</sup>) cell subsets. Mice were colonized with *H. hepaticus* for 5–6 weeks before analysis. Data summarize 3 independent experiments for *Rorc*<sup>ΔTreg</sup> ( $n=7$ ) and littermate controls (ctrl;  $n=7$  for **a**,  $n=6$  for **b**), and 4 independent experiments for *Maf*<sup>ΔTreg</sup> ( $n=10$ ) and littermate controls ( $n=8$ ). **c–e**, Co-transfer of *Maf*<sup>ΔTreg</sup> and control HH7-2tg T cells into wild-type *H. hepaticus*-colonized mice. **c**, Left, donor cell composition in the LILP of recipient mice. Right, ROR $\gamma$ t and FOXP3 expression in indicated donor-derived cells. **d**, Ratios of *Maf*<sup>ΔTreg</sup> (knockout, KO) versus control (WT) HH7-2tg donor-derived cells in the LILP. Dashed line represents ratio of co-transferred cells before transfer. **e**, Frequencies of T<sub>reg</sub> (FOXP3<sup>+</sup>) and TH17 (FOXP3<sup>-</sup>ROR $\gamma$ t<sup>+</sup>)

We next wished to determine whether ROR $\gamma$ t<sup>+</sup> T<sub>reg</sub> cells are critical for immune tolerance to gut pathogens. The transcription factor c-MAF attracted our attention as it was highly enriched in these cells<sup>11,17</sup> (Extended Data Fig. 6a) and known to promote an anti-inflammatory program, for example, IL-10 expression in other T helper cell subsets<sup>18,19</sup>. We therefore deleted *Maf* with *Foxp3*<sup>cre</sup> to test its function in T<sub>reg</sub> cells. In *H. hepaticus*-colonized *Maf*<sup>fl/fl</sup>; *Foxp3*<sup>cre</sup> (*Maf*<sup>ΔTreg</sup>) mice, despite incomplete depletion of c-MAF protein (Extended Data Fig. 6b), there was a marked decrease in the proportion of ROR $\gamma$ t<sup>+</sup> but not ROR $\gamma$ t<sup>-</sup> T<sub>reg</sub> cells among CD4<sup>+</sup> T cells in the large intestine, and a concomitant increase in TH17 cell frequency (Fig. 3a). *Maf*<sup>ΔTreg</sup> mice also had expanded numbers of total CD4<sup>+</sup> T cells in the large intestine, reflected by a pronounced accumulation of TH17 cells, but notably not ROR $\gamma$ t<sup>+</sup> T<sub>reg</sub> cells (Extended Data Fig. 6c). By contrast, after *H. hepaticus* colonization, TH17 cell expansion was less striking in *Rorc*<sup>fl/fl</sup>; *Foxp3*<sup>cre</sup> (*Rorc*<sup>ΔTreg</sup>) mice (Fig. 3a, Extended Data Fig. 6c), and neither a decrease of ROR $\gamma$ t<sup>+</sup> T<sub>reg</sub> cells nor an expansion of TH17 cells was observed in *Gata3*<sup>fl/fl</sup>; *Foxp3*<sup>cre</sup> (*Gata3*<sup>ΔTreg</sup>) mice (Extended Data Fig. 6d, e). The altered frequency of ROR $\gamma$ t<sup>+</sup> T<sub>reg</sub> and TH17 cell subsets led us to test whether the fate of *H. hepaticus*-specific T cells would be affected in the *Maf*<sup>ΔTreg</sup> and *Rorc*<sup>ΔTreg</sup> mice. Notably, HH-E2 tetramer<sup>+</sup> cells were predominantly TH17 in *Maf*<sup>ΔTreg</sup> mice, but mostly ROR $\gamma$ t<sup>+</sup> T<sub>reg</sub> in control mice (Fig. 3b, Extended Data Fig. 6f). By contrast, although

cells among donor-derived cells. Data are a summary of 10 mice from 2 independent experiments. **a, b, e**, Statistics were calculated by unpaired two-sided Welch's *t*-test. Error bars denote mean  $\pm$  s.d. *P* values are as follows: **a**, i =  $1.21 \times 10^{-6}$ , ii =  $8.82 \times 10^{-7}$ , iii = 0.016, iv =  $6.38 \times 10^{-4}$ , v =  $8.06 \times 10^{-4}$  and vi =  $9.89 \times 10^{-7}$ . **b**, i = 0.056, ii =  $7.48 \times 10^{-4}$ , iii =  $7.64 \times 10^{-7}$  and iv =  $6.01 \times 10^{-6}$ . **e**, i =  $6 \times 10^{-14}$ . NS = 0.86.

**f**, MA plot depicting RNA-seq comparison of donor naive T cell-derived *Maf*<sup>ΔTreg</sup> versus control FOXP3-YFP<sup>+</sup> iT<sub>reg</sub> cells (mean of two biologically independent experiments). Blue dots indicate 190 upregulated and 75 downregulated genes in the c-MAF-dependent signature. Highlighted blue dots represent downregulated genes related to T<sub>reg</sub> cell function, and highlighted red dots indicate genes that are also dependent on ROR $\gamma$ t<sup>11</sup>. Differentially expressed genes were calculated in DESeq2 using the Wald test with Benjamini–Hochberg correction to determine the false discovery rate (FDR) (FDR < 0.1 and log<sub>2</sub> fold change > 1.5).

*Rorc*<sup>ΔTreg</sup> mice also had an increased proportion of *H. hepaticus*-specific T<sub>reg</sub> cells, most tetramer<sup>+</sup> cells were T<sub>reg</sub> cells (Fig. 3b, Extended Data Fig. 6f). Collectively, these results suggest that pathobiont-specific ROR $\gamma$ t<sup>+</sup> iT<sub>reg</sub> cells are required for the suppression of inflammatory TH17 cell accumulation. Although ROR $\gamma$ t expression contributes to gut iT<sub>reg</sub> cell function, c-MAF has a more substantial role in the differentiation and/or function of these cells. *H. hepaticus*-specific T<sub>FH</sub> cell differentiation in the caecal patch did not seem to be affected in *Maf*<sup>ΔTreg</sup> mice (Extended Data Fig. 6g). Notably, as in IL-10-deficient mice, SFB-specific TH17 cells neither expanded nor adopted a TH1-like phenotype in *Maf*<sup>ΔTreg</sup> mice (Extended Data Fig. 6h, i). A potential explanation is that SFB- and *H. hepaticus*-specific TH17 responses are instructed by different innate immune pathways<sup>20,21</sup>.

To investigate how c-MAF regulates the gut ROR $\gamma$ t<sup>+</sup> iT<sub>reg</sub>–TH17 cell axis, we co-transferred equal numbers of naive *Maf*<sup>+/+</sup>; *Foxp3*<sup>cre</sup> (control) and *Maf*<sup>fl/fl</sup>; *Foxp3*<sup>cre</sup> HH7-2tg cells into *H. hepaticus*-colonized wild-type mice (Extended Data Fig. 7a, b). Two weeks after adoptive transfer, the *Maf*<sup>fl/fl</sup>; *Foxp3*<sup>cre</sup> HH7-2tg cells were markedly underrepresented compared to control cells in the LILP, mesenteric lymph nodes (mLNs) and spleen, and were unable to form iT<sub>reg</sub> cells (Fig. 3c–e and Extended Data Fig. 7c, d). Importantly, at homeostasis, mutant donor-derived cells did not give rise to a high frequency of TH17 cells (Fig. 3e). Transcriptomics analysis revealed that the c-MAF-deficient

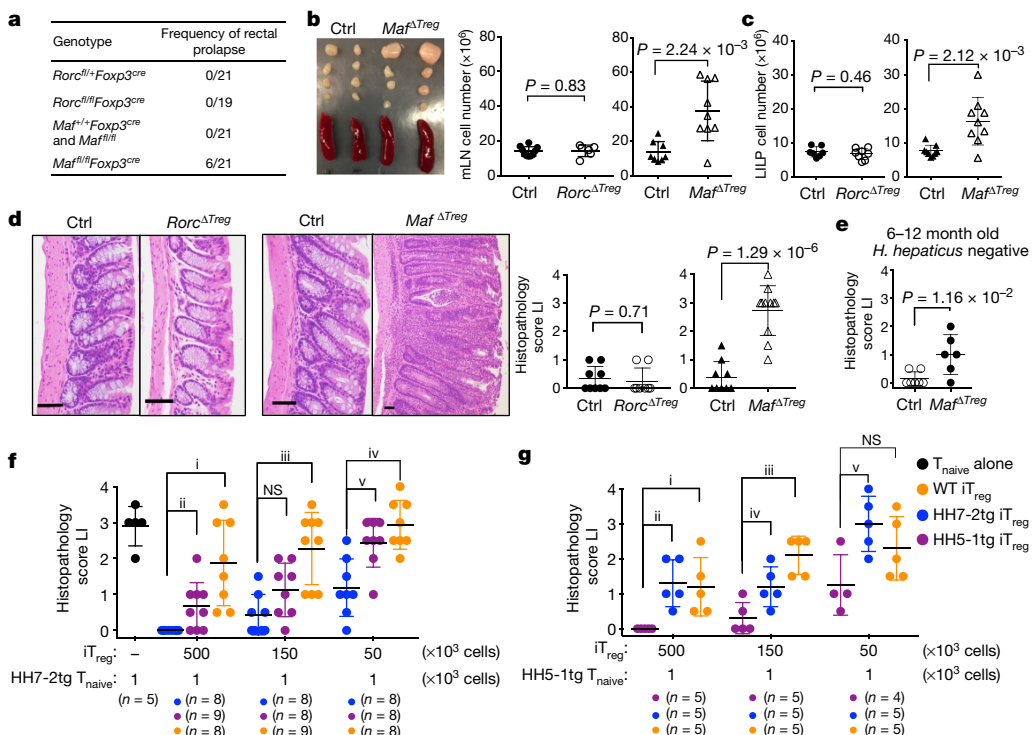


**Figure 4 | ROR $\gamma$ t<sup>+</sup> iT<sub>reg</sub> cells are required to maintain gut homeostasis.** **a**, Frequency of rectal prolapse by genotype. **b**, Left, spleens and mLNs from *Maf*<sup>ΔT<sub>reg</sub></sup> and littermate controls. Right, total cell numbers in mLNs. Data summarize three independent experiments for *Rorc*<sup>ΔT<sub>reg</sub></sup> ( $n=6$ ) and littermate controls ( $n=7$ ), and four independent experiments for *Maf*<sup>ΔT<sub>reg</sub></sup> ( $n=9$ ) and littermate controls ( $n=8$ ). **c**, Number of leukocytes in the LILP. Data summarize three independent experiments for *Rorc*<sup>ΔT<sub>reg</sub></sup> ( $n=7$ ) and littermate controls ( $n=8$ ), and four independent experiments for *Maf*<sup>ΔT<sub>reg</sub></sup> and littermate controls ( $n=9$ ). **d**, Representative histology of large intestine (LI) sections (left) and colitis scores (right) of mice with indicated genotypes. *Rorc*<sup>ΔT<sub>reg</sub></sup> ( $n=8$ ) and littermate controls ( $n=9$ ). *Maf*<sup>ΔT<sub>reg</sub></sup> ( $n=11$ ) and littermate controls ( $n=9$ ). Scale bars, 50  $\mu$ m.

iT<sub>reg</sub> cells were functionally impaired, as indicated by defective expression of *Il10* and other T<sub>reg</sub> cell signature genes, as well as of ROR $\gamma$ t-dependent genes<sup>11</sup> (Fig. 3f, Extended Data Fig. 7e–h). Taken together, these findings show that c-MAF is a crucial cell-intrinsic factor for both the generation and function of microorganism-specific iT<sub>reg</sub> cells. Notably, the vast majority of accumulated T<sub>H17</sub> cells in *Maf*<sup>ΔT<sub>reg</sub></sup> mice expressed c-MAF, indicating that the bulk of these cells did not arise from T<sub>reg</sub> cells in which c-MAF was deleted (Extended Data Fig. 7i). Thus, suppression of T<sub>H17</sub> cell expansion is mediated by these iT<sub>reg</sub> cells in *trans*.

ROR $\gamma$ t expression in iT<sub>reg</sub> cells has been implicated in the maintenance of gut immune homeostasis under different challenges<sup>11,12</sup>. However, spontaneous gut inflammation in *Rorc*<sup>ΔT<sub>reg</sub></sup> mice has not been described. We noticed that *Maf*<sup>ΔT<sub>reg</sub></sup>, but not *Rorc*<sup>ΔT<sub>reg</sub></sup> or control littermates, were prone to rectal prolapse (Fig. 4a). *Maf*<sup>ΔT<sub>reg</sub></sup> mice (8–12 weeks old) colonized with *H. hepaticus* for 5–6 weeks had enlarged large intestine-draining mLNs, and increased cellularity of mLNs and the large intestine (Fig. 4b, c). Histopathological analysis of the large intestine of these mice revealed mixed acute and chronic inflammation (Fig. 4d). Without *H. hepaticus* colonization, aged (6–12 months old) *Maf*<sup>ΔT<sub>reg</sub></sup> mice also exhibited mild spontaneous colitis (Fig. 4e). Notably, none of the above changes was observed in *Rorc*<sup>ΔT<sub>reg</sub></sup> mice (Fig. 4b–d). Thus, c-MAF but not ROR $\gamma$ t expression in iT<sub>reg</sub> cells is crucial for the suppression of spontaneous inflammation. Indeed, the transcriptional profile of *H. hepaticus*-specific T effector (T<sub>eff</sub>) cells from *Maf*<sup>ΔT<sub>reg</sub></sup> mice with spontaneous colitis was highly similar to that of pathogenic T<sub>H17</sub> cells in IL-10RA blockade-induced

e, Colitis scores in aged *H. hepaticus*-negative *Maf*<sup>ΔT<sub>reg</sub></sup> ( $n=6$ ) and littermate control ( $n=7$ ) mice. **f, g**, Suppression of *H. hepaticus*-specific TCRtg cell-mediated transfer colitis by *in vitro* differentiated iT<sub>reg</sub> cells. Data summarize two independent experiments with indicated sample size ( $n$ ) in total. Colitis scores for *Rag1*<sup>−/−</sup> mice that received the indicated TCRtg naive T cells and iT<sub>reg</sub> combinations. All statistics were calculated by unpaired two-sided Welch's *t*-test. Error bars denote mean  $\pm$  s.d. *P* values are indicated on the figure or as follows: **f**, i =  $5.34 \times 10^{-4}$ , ii =  $1.24 \times 10^{-2}$ , iii =  $3.64 \times 10^{-4}$ , iv =  $3.26 \times 10^{-4}$  and v =  $4.54 \times 10^{-3}$ . NS = 0.056. **g**, i = 0.013, ii =  $2.50 \times 10^{-3}$ , iii =  $4.59 \times 10^{-4}$ , iv = 0.024, and v = 0.016. NS = 0.12.

colitis, but differed markedly from homeostatic T<sub>H17</sub> cells (which are predominantly SFB-specific) (Extended Data Fig. 8a–f).

Similar to the *Maf*<sup>ΔT<sub>reg</sub></sup> strain, mice with inactivation of STAT3 in the T<sub>reg</sub> compartment or impaired TGF $\beta$  signalling in CD4 $^{+}$  T cells also lacked ROR $\gamma$ t<sup>+</sup> T<sub>reg</sub> cells and developed spontaneous colitis<sup>12,22,23</sup> (Extended Data Fig. 9a, b). Consistent with these findings, c-MAF expression in T<sub>reg</sub> cells required a combination of both TGF $\beta$  and STAT3 signals *in vitro* and *in vivo*, as it does in other CD4 $^{+}$  T cells<sup>18,19</sup> (Extended Data Fig. 9a–c). This suggests that c-MAF integrates anti-inflammatory TGF $\beta$  receptor signals with microorganism-induced cytokine-dependent STAT3 activation to mediate ROR $\gamma$ t<sup>+</sup> T<sub>reg</sub> induction.

Although c-MAF is also expressed, albeit at a lower level, in nT<sub>reg</sub> cells, c-MAF-deficient and -sufficient nT<sub>reg</sub> cells showed equivalent activity in inhibiting T<sub>eff</sub> cell proliferation *in vitro*, as well as in suppressing pathogenesis in a model of T cell transfer colitis *in vivo* (Extended Data Fig. 10a, b). We therefore wondered why, despite their increased numbers (Extended Data Fig. 6c), nT<sub>reg</sub> cells were not sufficient to establish gut homeostasis in *Maf*<sup>ΔT<sub>reg</sub></sup> mice. Adoptive transfer of 1,000 naive HH7-2tg or HH5-1tg cells into *H. hepaticus*-colonized *Rag1*<sup>−/−</sup> mice led to colitis. Taking advantage of this system, we compared the suppressive function of iT<sub>reg</sub> cells differentiated *in vitro* from naive HH7-2tg, HH5-1tg and polyclonal T cells. We found that epitope-specific iT<sub>reg</sub> were better at suppressing colitis, providing a potential explanation for why pathobiont-specific iT<sub>reg</sub> cells are required in addition to nT<sub>reg</sub> cells to maintain gut homeostasis<sup>24</sup> (Fig. 4f, g).

Our results reveal a mechanism for how a healthy individual can host a ‘two-faced’ commensal pathobiont such as *H. hepaticus* without developing inflammatory disease. Our findings suggest that T<sub>reg</sub> cell induction serves as a strategy to establish commensalism, not only by helping the microorganisms to colonize their niche<sup>25</sup>, but also by protecting the host from inflammation. A similar requirement for iT<sub>reg</sub> cells has also been reported in the establishment of food tolerance<sup>26</sup>. Our observations in *Maf*<sup>ΔTreg</sup> mice are linked to and help explain the expansion of colitogenic T<sub>H</sub>17 cells in mice with T<sub>reg</sub>-specific inactivation of STAT3<sup>23</sup>. Like c-MAF, STAT3 is probably required for the differentiation and/or function of microbiota-induced ROR $\gamma$ <sup>+</sup> iT<sub>reg</sub> cells<sup>12</sup>. Moreover, microorganism-specific iT<sub>reg</sub> cells, compared with non-specific nT<sub>reg</sub> cells, can better suppress inflammatory T<sub>eff</sub> cells by recognizing the same epitopes. This result raises the prospect of harnessing the mechanisms of pathobiont-specific iT<sub>reg</sub> cell responses to re-establish homeostasis in patients with inflammatory bowel disease, for example, by engineering non-pathogenic T<sub>reg</sub> cell-inducing microorganisms<sup>27</sup> to express pathobiont antigens.

**Online Content** Methods, along with any additional Extended Data display items and Source Data, are available in the online version of the paper; references unique to these sections appear only in the online paper.

Received 20 April 2017; accepted 2 January 2018.

Published online 7 February 2018.

1. Round, J. L. & Mazmanian, S. K. The gut microbiota shapes intestinal immune responses during health and disease. *Nat. Rev. Immunol.* **9**, 313–323 (2009).
2. Hooper, L. V., Littman, D. R. & Macpherson, A. J. Interactions between the microbiota and the immune system. *Science* **336**, 1268–1273 (2012).
3. Kamada, N., Seo, S. U., Chen, G. Y. & Núñez, G. Role of the gut microbiota in immunity and inflammatory disease. *Nat. Rev. Immunol.* **13**, 321–335 (2013).
4. Chow, J., Tang, H. & Mazmanian, S. K. Pathobionts of the gastrointestinal microbiota and inflammatory disease. *Curr. Opin. Immunol.* **23**, 473–480 (2011).
5. Kullberg, M. C. et al. IL-23 plays a key role in *Helicobacter hepaticus*-induced T cell-dependent colitis. *J. Exp. Med.* **203**, 2485–2494 (2006).
6. Hue, S. et al. Interleukin-23 drives innate and T cell-mediated intestinal inflammation. *J. Exp. Med.* **203**, 2473–2483 (2006).
7. Sanderson, S., Campbell, D. J. & Shastri, N. Identification of a CD4<sup>+</sup> T cell-stimulating antigen of pathogenic bacteria by expression cloning. *J. Exp. Med.* **182**, 1751–1757 (1995).
8. Yang, Y. et al. Focused specificity of intestinal T<sub>H</sub>17 cells towards commensal bacterial antigens. *Nature* **510**, 152–156 (2014).
9. Kearney, E. R., Pape, K. A., Loh, D. Y. & Jenkins, M. K. Visualization of peptide-specific T cell immunity and peripheral tolerance induction *in vivo*. *Immunity* **1**, 327–339 (1994).
10. Moon, J. J. et al. Naive CD4<sup>+</sup> T cell frequency varies for different epitopes and predicts repertoire diversity and response magnitude. *Immunity* **27**, 203–213 (2007).
11. Sefik, E. et al. Individual intestinal symbionts induce a distinct population of ROR $\gamma$ <sup>+</sup> regulatory T cells. *Science* **349**, 993–997 (2015).
12. Ohnmacht, C. et al. The microbiota regulates type 2 immunity through ROR $\gamma$ <sup>+</sup> T cells. *Science* **349**, 989–993 (2015).
13. Schiering, C. et al. The alarmin IL-33 promotes regulatory T-cell function in the intestine. *Nature* **513**, 564–568 (2014).
14. Hirota, K. et al. Fate mapping of IL-17-producing T cells in inflammatory responses. *Nat. Immunol.* **12**, 255–263 (2011).
15. Hand, T. W. et al. Acute gastrointestinal infection induces long-lived microbiota-specific T cell responses. *Science* **337**, 1553–1556 (2012).
16. Chai, J. N. et al. *Helicobacter* species are potent drivers of colonic T cell responses in homeostasis and inflammation. *Sci. Immunol.* **2**, eaal5068 (2017).
17. Yang, B. H. et al. Foxp3<sup>+</sup> T cells expressing ROR $\gamma$ t represent a stable regulatory T-cell effector lineage with enhanced suppressive capacity during intestinal inflammation. *Mucosal Immunol.* **9**, 444–457 (2016).
18. Ciofani, M. et al. A validated regulatory network for Th17 cell specification. *Cell* **151**, 289–303 (2012).
19. Apetoh, L. et al. The aryl hydrocarbon receptor interacts with c-Maf to promote the differentiation of type 1 regulatory T cells induced by IL-27. *Nat. Immunol.* **11**, 854–861 (2010).
20. Hoshi, N. et al. MyD88 signalling in colonic mononuclear phagocytes drives colitis in IL-10-deficient mice. *Nat. Commun.* **3**, 1120 (2012).
21. Ivanov, I. I. et al. Specific microbiota direct the differentiation of IL-17-producing T-helper cells in the mucosa of the small intestine. *Cell Host Microbe* **4**, 337–349 (2008).
22. Gorelik, L. & Flavell, R. A. Abrogation of TGF $\beta$  signaling in T cells leads to spontaneous T cell differentiation and autoimmune disease. *Immunity* **12**, 171–181 (2000).
23. Chaudhry, A. et al. CD4<sup>+</sup> regulatory T cells control T<sub>H</sub>17 responses in a Stat3-dependent manner. *Science* **326**, 986–991 (2009).
24. Haribhai, D. et al. A requisite role for induced regulatory T cells in tolerance based on expanding antigen receptor diversity. *Immunity* **35**, 109–122 (2011).
25. Round, J. L. et al. The Toll-like receptor 2 pathway establishes colonization by a commensal of the human microbiota. *Science* **332**, 974–977 (2011).
26. Kim, K. S. et al. Dietary antigens limit mucosal immunity by inducing regulatory T cells in the small intestine. *Science* **351**, 858–863 (2016).
27. Atarashi, K. et al. T<sub>reg</sub> induction by a rationally selected mixture of Clostridia strains from the human microbiota. *Nature* **500**, 232–236 (2013).

**Supplementary Information** is available in the online version of the paper.

**Acknowledgements** We thank S. Y. Kim and the NYU Rodent Genetic Engineering Laboratory (RGEL) for generating TCR transgenic mice, A. Heguy and colleagues at the NYU School of Medicine’s Genome Technology Center (GTC) for preparation of RNA-seq libraries and RNA sequencing, the NIH Tetramer Core Facility for generating MHC class II tetramers, K. Murphy for providing the 58 $\alpha$ <sup>+</sup> $\beta$ <sup>+</sup> hybridoma line, D. E. Levy for providing the *Stat3*<sup>fl/fl</sup>; *Cd4*<sup>cre</sup> mice, J. Fox for providing the *H. hepaticus* strain, P. Dash and P. G. Thomas for advice on single-cell TCR cloning, and J. A. Hall, J. Muller and J. Lafaille for suggestions on the manuscript. The Experimental Pathology Research Laboratory of NYU Medical Center is supported by National Institutes of Health Shared Instrumentation grants S10OD010584-01A1 and S10OD018338-01. The GTC is partially supported by the Cancer Center Support grant P30CA016087 at the Laura and Isaac Perlmutter Cancer Center. This work was supported by the Irvington Institute fellowship program of the Cancer Research Institute (M.X.); the training program in Immunology and Inflammation 5T32AI100853 (M.P.); the Helen and Martin Kimmel Center for Biology and Medicine (D.R.L.); the Colton Center for Autoimmunity (D.R.L.); and National Institutes of Health grant R01DK103358 (R.B. and D.R.L.). D.R.L. is an Investigator of the Howard Hughes Medical Institute.

**Author Contributions** M.X. and M.P. designed and performed all experiments and analysed the data. Y.D. performed blinded histology scoring on colitis sections. C.A. and C.G. assisted with *in vivo* and *in vitro* experiments. R.Y. and M.P. performed RNA-seq analysis. O.J.H. and Y.B. analysed the *Gata3*<sup>ΔTreg</sup> mouse phenotype. R.B. supervised RNA-seq analysis. M.X., M.P. and D.R.L. wrote the manuscript with input from the co-authors. D.R.L. supervised the research and contributed to experimental design.

**Author Information** Reprints and permissions information is available at [www.nature.com/reprints](http://www.nature.com/reprints). The authors declare no competing financial interests. Readers are welcome to comment on the online version of the paper. Publisher’s note: Springer Nature remains neutral with regard to jurisdictional claims in published maps and institutional affiliations. Correspondence and requests for materials should be addressed to D.R.L. (dan.littman@med.nyu.edu).

**Reviewer Information** *Nature* thanks C. Ohnmacht and the other anonymous reviewer(s) for their contribution to the peer review of this work.

## METHODS

**Mice.** Mice were bred and maintained in the animal facility of the Skirball Institute (New York University School of Medicine) and the National Institute of Allergy and Infectious Diseases (NIAID) in specific pathogen-free conditions. C57BL/6 mice were obtained from Jackson Laboratories or Taconic Farm. *Il10<sup>-/-</sup>* (B6.129P2-*Il10<sup>tm1Cgn</sup>*/J) mice were purchased from Jackson Laboratories and bred with wild-type C57BL/6 mice, which subsequently generated *Il10<sup>+/+</sup>* and *Il10<sup>-/-</sup>* littermates by heterozygous breeding. CD4-dnTGFbRII mice<sup>22</sup> were purchased from Jackson Laboratories, and bred with wild-type C57BL/6 mice to generate CD4-dnTGFbRII and wild-type littermates. *Cd4<sup>cre</sup>* (*Tg(Cd4-cre)1Cwi/Bflu*) and *Cd45.1* (B6.SJL-*Ptprc**Pcpb/BoJ*) mice were purchased from Jackson Laboratories. *Foxp3<sup>creYFP</sup>* mice were previously described and obtained from Jackson Laboratories<sup>28</sup>. *Il23<sup>gfp</sup>* and *Maf<sup>gfl</sup>* strains were previously described<sup>29,30</sup> and provided by M. Oukka and C. Birchmeier, respectively. *Stat3<sup>fl/fl</sup>;Cd4<sup>cre</sup>* mice were provided by D. E. Levy. *Gata3<sup>fl/fl</sup>;Foxp3<sup>creYFP</sup>* mice were bred at the NIAID. Littermates with matched sex (both males and females) were used. Except the aged mice (6–12 months old) analysed in the experiments of Fig. 4e, mice in all the experiments were 6–12 weeks old at the starting point of treatments. Animal sample size estimates were determined using power analysis (power = 90% and  $\alpha = 0.05$ ) based on the mean and standard deviation from our previous studies and/or pilot studies using 4–5 mice per group. All animal procedures were performed in accordance with protocols approved by the Institutional Animal Care and Usage Committee of New York University School of Medicine or the NIAID as applicable.

**Antibodies, intracellular staining and flow cytometry.** The following monoclonal antibodies were purchased from eBiosciences, BD Pharmingen or BioLegend: CD3 (145-2C11), CD4 (RM4-5), CD25 (PC61), CD44 (IM7), CD45.1 (A20), CD45.2 (104), CD62L (MEL-14), CXCR5 (L138D7), NPR-1 (3E12), ST2 (RMST2-2), TCR $\beta$  (H57-597), TCR V $\beta$ 6 (RR4-7), TCR V $\beta$ 8.1/8.2 (MR5-2), TCR V $\beta$ 14 (14-2), BCL6 (K112-91), c-MAF (T54-853), FOXP3 (FJK-16s), GATA3 (TWAJ), Helios (22F6), ROR $\gamma$ t (B2D or Q31-378), T-bet (eBio4B10), IL-10 (JES5-16E3), IL-17A (eBio17B7) and IFN $\gamma$  (XM61.2). 4',6-diamidino-2-phenylindole (DAPI) or Live/dead fixable blue (ThermoFisher) was used to exclude dead cells.

For transcription factor staining, cells were stained for surface markers, followed by fixation and permeabilization before nuclear factor staining according to the manufacturer's protocol (FOXP3 staining buffer set from eBioscience). For cytokine analysis, cells were incubated for 5 h in RPMI with 10% FBS, phorbol 12-myristate 13-acetate (PMA) (50 ng ml $^{-1}$ ; Sigma), ionomycin (500 ng ml $^{-1}$ ; Sigma) and GolgiStop (BD). Cells were stained for surface markers before fixation and permeabilization, and then subjected to intracellular cytokine staining according to the manufacturer's protocol (Cytofix/Cytoperm buffer set from BD Biosciences).

Flow cytometric analysis was performed on an LSR II (BD Biosciences) or an Aria II (BD Biosciences) and analysed using FlowJo software (Tree Star).

**Isolation of lymphocytes.** Intestinal tissues were sequentially treated with PBS containing 1 mM DTT at room temperature for 10 min, and 5 mM EDTA at 37°C for 20 min to remove epithelial cells, and then minced and dissociated in RPMI containing collagenase (1 mg ml $^{-1}$  collagenase II; Roche), DNase I (100  $\mu$ g ml $^{-1}$ ; Sigma), dispase (0.05 U ml $^{-1}$ ; Worthington) and 10% FBS with constant stirring at 37°C for 45 min (small intestine) or 60 min (large intestine). Leukocytes were collected at the interface of a 40%/80% Percoll gradient (GE Healthcare). The Peyer's patches and caecal patch were treated in a similar fashion except for the first step of removal of epithelial cells. Lymph nodes and spleens were mechanically disrupted.

**Single-cell TCR cloning.** *Il23<sup>gfp/+</sup>* mice were maintained in SFB-free conditions to guarantee low T $_H$ 17 background levels. To induce a robust T $_H$ 17 cell response, the mice were orally infected with *H. hepaticus* and injected intraperitoneally with 1 mg anti-IL-10RA (clone 1B1.3A, Bioxcell) every week from the day of infection. After two weeks, large intestine GFP $^+$  CD4 $^+$  T cells were sorted on the BD Aria II and deposited at one cell per well into 96-well PCR plates pre-loaded with 5  $\mu$ l high-capacity cDNA reverse transcription mix (Thermo Fisher) supplemented with 0.1% Triton X-100 (Sigma-Aldrich). Immediately after sorting, whole plates were incubated at 37°C for 2 h, and then inactivated at 85°C for 10 min for cDNA preparation. A nested multiplex PCR approach described previously was used to amplify the CDR3 $\alpha$  and CDR3 $\beta$  TCR regions separately from the single cell cDNA<sup>31</sup>. PCR products were cleaned up with ExoSap-IT reagent (USB) and Sanger sequencing was performed by Macrogen. Open reading frame nucleotide sequences of the TCR $\alpha$  and TCR $\beta$  families were retrieved from the IMGT database (<http://www.imgt.org>)<sup>32</sup>.

**Generation of TCR hybridomas.** The NFAT-GFP 58 $\alpha$ - $\beta$ - hybridoma cell line was provided by K. Murphy<sup>33</sup>. To reconstitute TCRs, cDNA of TCR $\alpha$  and TCR $\beta$  were synthesized as gBlocks fragments by Integrated DNA Technologies (IDT), linked with the self-cleavage sequence of 2A (TCR $\alpha$ -p2A-TCR $\beta$ ), and shuttled into a modified MigR1 retrovector in which IRES-GFP was replaced with IRES-mCD4 (mouse CD4) as described previously<sup>8</sup>. Then retroviral vectors were transfected

into Phoenix E packaging cells using TransIT-293 (Mirus). Hybridoma cells were transduced with viral supernatants in the presence of polybrene (8  $\mu$ g ml $^{-1}$ ) by spin infection for 90 min at 32°C. Transduction efficiencies were monitored by checking mCD3 surface expression three days later.

**Assay for hybridoma activation.** Splenic dendritic cells were used as antigen-presenting cells (APCs). B6 mice were injected intraperitoneally with 5  $\times$  10 $^6$  FLT3L-expressing B16 melanoma cells to drive APC proliferation as previously described<sup>34</sup>. Splenocytes were prepared 10 days after injection, and positively enriched for CD11c $^+$  cells using MACS LS columns (Miltenyi). 2  $\times$  10 $^4$  hybridoma cells were incubated with 10 $^5$  APCs and antigens in round bottom 96-well plates for two days. GFP induction in the hybridomas was analysed by flow cytometry as an indicator of TCR activation.

**Construction and screen of whole-genome shotgun library of *H. hepaticus*.** The shotgun library was prepared with a procedure modified from previous studies<sup>7,8</sup>. In brief, genomic DNA was purified from cultured *H. hepaticus* with DNeasy PowerSoil kit (Qiagen). DNA was partially digested with MluCI (NEB), and the fraction between 500 and 2,000 base pairs (bp) was ligated into the EcoRI-linearized pGEX-6P-1 expression vector (GE Healthcare). Ligation products were transformed into ElectroMAX DH10B competent Cells (Invitrogen) by electroporation. To estimate the size of the library, we cultured 1% and 0.1% of transformed bacteria on lysogeny broth (LB) agar plates containing 100  $\mu$ g ml $^{-1}$  Ampicillin for 12 h and then quantified the number of colonies. The library is estimated to contain 3  $\times$  10 $^4$  clones. To ensure the quality of the library, we sequenced the inserts of randomly picked colonies. All the sequences were mapped to the *H. hepaticus* genome, and their sizes were 700 to 1,200 bp. We aliquoted the bacteria into 96-well deepwell plates (Axygen) (~30 clones per well) and grew with AirPort microporous cover (Qiagen) in 37°C. The expression of exogenous proteins was induced by 1 mM isopropylthiogalactoside (IPTG, Sigma) for 4 h. Then bacteria were collected in PBS and heat-killed by incubating at 85°C for 1 h, and stored at –20°C until use. Two screening rounds were performed to identify the antigen-expressing clones. For the first round, pools of heat-killed bacterial clones were added to a co-culture of splenic APCs and hybridomas. Clones within the positive pools were subsequently screened individually against the hybridoma bait. Finally, the inserts of positive clones were subjected to Sanger sequencing. The sequences were blasted against the genome sequence of *H. hepaticus* (ATCC51449) and aligned to the annotated open reading frames. Full-length open reading frames containing the retrieved fragments were cloned into pGEX-6P-1 to confirm their activity in the T cell stimulation assay.

**Epitope mapping.** We cloned overlapping fragments spanning the entire HH\_1713 coding region into the pGEX-6P-1 expression vector, and expressed these in *Escherichia coli* BL21 cells. The heat-killed bacteria were used to stimulate relevant hybridomas. This process was repeated until we mapped the epitope to a region containing 30 amino acids. The potential MHC class II epitopes were predicted with online software RANKPEP<sup>35</sup>. Overlapping peptides spanning the predicted region were further synthesized (Genescrypt) and verified by stimulation of the hybridomas.

**Generation of TCRtg mice.** TCR sequences of HH5-1 and HH7-2 were cloned into the pT $\alpha$  and pT $\beta$  vectors provided by D. Mathis<sup>36</sup>. TCR transgenic mice were generated by the Rodent Genetic Engineering Core at the New York University School of Medicine. Positive pups were genotyped by testing TCR V $\beta$ 8.1/8.2 (HH5-1tg) or V $\beta$ 6 (HH7-2tg) expression on T cells from peripheral blood.

**MHC class II tetramer production and staining.** HH-E2 tetramer was produced by the NIH Tetramer Core Facility<sup>37</sup>. In brief, QESPRIAAAYTIKGA (HH\_1713-E2), an immunodominant epitope validated with the hybridoma stimulation assay, was covalently linked to I-A $b$  via a flexible linker, to produce pMHCII monomers. Soluble monomers were purified, biotinylated, and tetramerized with phycoerythrin- or allophycocyanin-labelled streptavidin. SFB-specific tetramer (3340-A6 tetramer) was described previously<sup>8</sup>. To stain endogenous T cells, mononuclear cells from SLIP, LILP or caecal patch were first resuspended in MACS buffer with FcR block, 2% mouse serum and 2% rat serum. Then tetramer was added (10 nM) and incubated at room temperature for 60 min, and cells were re-suspended by pipetting every 20 min. Cells were washed with MACS buffer and followed by regular surface marker staining at 4°C.

**Adoptive transfer of TCRtg cells.** Recipient mice were colonized with *H. hepaticus* and/or SFB by oral gavage seven days before adoptive transfer (The method for oral infection of SFB has been previously described<sup>18</sup>). Spleens from donor TCRtg mice were collected and mechanically disassociated. Red blood cells were lysed using ACK lysis buffer (Lonza). For TCRtg mice in wild-type background, naive Tg T cells were sorted as CD4 $^+$ CD3 $^+$ CD44 $^{lo}$ CD62L $^{hi}$ CD25 $^-$ V $\beta$ 6 $^+$  (HH7-2tg), V $\beta$ 8.1/8.2 $^+$  (HH5-1tg) or V $\beta$ 14 $^+$  (7B8tg) on the Aria II (BD Biosciences). For HH7-2tg mice bred to the *Foxp3<sup>creYFP</sup>* background, naive transgenic T cells were sorted as CD4 $^+$ CD3 $^+$ CD44 $^{lo}$ CD62L $^{hi}$ FOXP3 $^{CreYFP}$ V $\beta$ 6 $^+$ . Cells were resuspended in PBS on ice and transferred into congenic isotype-labelled recipient mice by retro-orbital injection. Cells from indicated tissues were analysed two weeks after transfer.

**H. hepaticus culture and oral infection.** *H. hepaticus* was provided by J. Fox (MIT). Frozen stock aliquots of *H. hepaticus* were stored in Brucella broth with 20% glycerol and frozen at -80°C. The bacteria were grown on blood agar plates (TSA with 5% sheep blood, Thermo Fisher). Inoculated plates were placed into a hypoxia chamber (Billups-Rothenberg), and anaerobic gas mixture consisting of 80% nitrogen, 10% hydrogen, and 10% carbon dioxide (Airgas) was added to create a micro-aerobic atmosphere, in which the oxygen concentration was 3–5%. The micro-aerobic jars containing bacterial plates were left at 37°C for 5 days before animal inoculation. For oral infection, *H. hepaticus* was resuspended in Brucella broth by application of a pre-moistened sterile cotton swab applicator tip to the colony surface. The concentration of bacterial inoculation dose was determined by the use of a spectrophotometric optical density (OD) analysis at 600 nm, and adjusted to OD<sub>600 nm</sub> readings between 1 and 1.5. 0.2 ml bacterial suspension was administered to each mouse by oral gavage. Mice were inoculated every 5 days for a total of two doses.

**H. hepaticus-specific TCRtg cell-mediated transfer colitis.** Naive T ( $T_{naive}$ ) cells were isolated from the spleens of HH7-2tg mice as CD4<sup>+</sup>CD3<sup>+</sup>CD44<sup>lo</sup>CD62L<sup>hi</sup>CD25<sup>-</sup>Vβ3<sup>+</sup> by FACS. The sorted cells ( $1 \times 10^3$ ) were administered by retro-orbital injection into *H. hepaticus*-colonized *Rag1*<sup>-/-</sup> mice. After two weeks, cells from the large intestine were isolated and analysed by flow cytometry.

**C. rodentium-mediated colon inflammation.** *C. rodentium* strain DBS100 (ATCC51459; American Type Culture Collection) was used for all inoculations. Bacteria were grown at 37°C in LB broth to OD<sub>600 nm</sub> reading between 0.4 and 0.6. Mice were inoculated with 200 µl of a bacterial suspension ( $1 \times 10^9$ – $2 \times 10^9$  colony-forming units (CFU)) by way of oral gavage. After 15 days, cells from the large intestine were isolated, stained for HH-E2 tetramer and other markers as indicated and analysed by flow cytometry.

**DSS-induced colitis.** Mice were colonized with *H. hepaticus* 5 days before DSS treatment. To induce colitis, mice were given 2% DSS (50,000MW, Affymetrix/USB) in drinking water for 2 cycles, with each exposure for 7 days with 5 days of untreated water in between. Control mice were given drinking water for the same period. Cells from the large intestine were then isolated, stained for HH-E2 tetramer and other marks as indicated and analyzed by flow cytometry. Animal weights were monitored daily during the entire experiment.

**T cell culture.** Naive CD4<sup>+</sup> T cells were purified from spleen and lymph nodes of mice with indicated genotypes. In brief, CD4<sup>+</sup> T cells were positively selected from organ cell suspensions by magnetic-activated cell sorting using CD4 beads (MACS, Miltenyi) according to the product protocol, and then isolated as CD4<sup>+</sup>CD3<sup>+</sup>CD44<sup>lo</sup>CD62L<sup>hi</sup>CD25<sup>-</sup> (polyclonal) or CD4<sup>+</sup>CD3<sup>+</sup>CD44<sup>lo</sup>CD62L<sup>hi</sup>CD25<sup>-</sup>Vβ3<sup>+</sup> (HH7-2tg) or Vβ38.1/8.2<sup>+</sup> (HH5-1tg) by FACS. T cells were cultured at 37°C in RPMI (Hyclone) supplemented with 10% heat-inactivated FBS (Hyclone), 50 U penicillin-streptomycin (Hyclone), 2 mM glutamine (Hyclone), 10 mM HEPES (Hyclone), 1 mM sodium pyruvate (Hyclone) and 50 µM β-mercaptoethanol (Gibco).

To generate iT<sub>reg</sub> cells for transfer colitis experiments (see below), wild-type, HH7-2tg or HH5-1tg cells were seeded at  $1 \times 10^6$  cells in 1.5 ml per well in 12-well plates pre-coated with an anti-hamster IgG secondary antibody (MP Biomedicals), and cultured for 72 h. The culture was supplemented with soluble anti-CD3ε (0.25 µg ml<sup>-1</sup>, Bioxcell, clone 145-2C11) and anti-CD28 (1 µg ml<sup>-1</sup>, Bioxcell, clone 37.51) for TCR stimulation, and anti-IL-4 (1 µg ml<sup>-1</sup>, Bioxcell, clone 11B11), anti-IFNγ (1 µg ml<sup>-1</sup>, Bioxcell, clone XMG1.2), human TGFβ1 (20 ng ml<sup>-1</sup>, Peprotech), human IL-2 (500 U ml<sup>-1</sup>, Peprotech) and all-trans retinoic acid (100 nM, sigma) for optimal iT<sub>reg</sub> cell polarization. Aliquots of cultured cells were analysed for intracellular FOXP3 staining by flow cytometry. After they were confirmed to be more than 98% FOXP3<sup>+</sup>, the remaining live cells (DAPI negative) were FACS sorted for adoptive transfer.

To test the conditions inducing c-MAF expression, 200 µl naive T cells isolated from *Maf*<sup>fl/fl</sup>, *Maf*<sup>fl/fl</sup>; *Cd4*<sup>cre</sup> or *Stat3*<sup>fl/fl</sup>; *Cd4*<sup>cre</sup> mice were seeded at  $1 \times 10^5$  cells per well in 96-well plates pre-coated with the anti-hamster IgG secondary antibody, and cultured for 48 h. The culture was supplemented with soluble anti-CD3ε (0.25 µg ml<sup>-1</sup>) and anti-CD28 (1 µg ml<sup>-1</sup>) for TCR stimulation. Combinations of the following antibodies or cytokines were added as indicated in Extended Data Fig. 9c: anti-TGFβ (1 µg ml<sup>-1</sup>, Bioxcell, 1D11.16.8), human TGFβ1 (0.3 or 20 ng ml<sup>-1</sup>, Peprotech), human IL-2 (500 U ml<sup>-1</sup>, Peprotech), mouse IL-6 (20 ng ml<sup>-1</sup>, Thermo), mouse IL-10 (100 ng ml<sup>-1</sup>, Peprotech), mouse IL-27 (25 ng ml<sup>-1</sup>, Thermo), mouse IL-12 (10 ng ml<sup>-1</sup>, Peprotech), mouse IL-1β (10 ng ml<sup>-1</sup>, Peprotech), mouse IL-4 (10 ng ml<sup>-1</sup>, R&D systems), mouse IFNγ (10 ng ml<sup>-1</sup>, Peprotech), and all-trans retinoic acid (100 nM, sigma).

**T<sub>reg</sub> cell *in vitro* suppression assay.**  $T_{naive}$  cells with the phenotype CD4<sup>+</sup>CD3<sup>+</sup>CD44<sup>lo</sup>CD62L<sup>hi</sup>CD25<sup>-</sup> were isolated from the spleen and lymph nodes of CD45.1 wild-type B6 mice by FACS and labelled with carboxyfluorescein diacetate succinimidyl ester (CFSE). iT<sub>reg</sub> (CD45.2) cells with the phenotype

CD4<sup>+</sup>CD3<sup>+</sup>FOXP3<sup>creYFP</sup><sup>+</sup>NRP1<sup>+</sup> were isolated from the spleen and lymph nodes of *Foxp3*<sup>creYFP</sup> or *Maf*<sup>ΔTreg</sup> mice by FACS. B cells were isolated from the spleen and lymph nodes of CD45.2 wild-type B6 mice by positive enrichment for B220<sup>+</sup> cells using MACS LS columns (Miltenyi).  $2.5 \times 10^4$  CFSE-labelled  $T_{naive}$  cells were cultured for 72 h with B cell APCs ( $5 \times 10^4$ ) and anti-CD3 (1 µg ml<sup>-1</sup>) in the presence or absence of various numbers of iT<sub>reg</sub> cells as indicated. The cell division index of responder T cells was assessed by dilution of CFSE using FlowJo software (Tree Star).

**Suppression of adoptive transfer colitis with iT<sub>reg</sub> cells.** To compare the suppressive function of c-MAF-sufficient and -deficient iT<sub>reg</sub> cells, CD4<sup>+</sup>CD3<sup>+</sup>CD25<sup>-</sup>CD45RB<sup>hi</sup> T<sub>eff</sub> cells were isolated by FACS from B6 mouse spleens and CD4<sup>+</sup>CD3<sup>+</sup>FOXP3-YFP<sup>+</sup>NRP1<sup>+</sup> iT<sub>reg</sub> were isolated from spleen of *H. hepaticus*-colonized *Foxp3*<sup>creYFP</sup> or *Maf*<sup>ΔTreg</sup> mice. T<sub>eff</sub> cells ( $5 \times 10^5$ ) were administered by retro-orbital injection into *H. hepaticus*-colonized *Rag1*<sup>-/-</sup> mice alone, or simultaneously with  $4 \times 10^5$  iT<sub>reg</sub> cells as previously described<sup>38</sup>. Animal weights were measured weekly.

To compare the suppressive function of TCRtg and polyclonal iT<sub>reg</sub> cells,  $T_{naive}$  cells with the phenotype CD4<sup>+</sup>CD3<sup>+</sup>CD44<sup>lo</sup>CD62L<sup>hi</sup>CD25<sup>-</sup> and Vβ3<sup>+</sup> (HH7-2tg) or CD4<sup>+</sup>CD3<sup>+</sup>CD44<sup>lo</sup>CD62L<sup>hi</sup>CD25<sup>-</sup> and Vβ38.1/8.2<sup>+</sup> (HH5-1tg) were isolated from spleens of TCRtg mice. 1,000 naive HH7-2tg or HH5-1tg cells were co-transferred with different numbers (500,000, 150,000 or 50,000 as indicated in Fig. 4f, g) of *in vitro* polarized (see T cell culture, above) HH7-2tg, HH5-1tg or polyclonal iT<sub>reg</sub> cells into *H. hepaticus*-colonized *Rag1*<sup>-/-</sup> mice by retro-orbital injection.

Co-housed littermate recipients were randomly assigned to different treatment groups such that each cage contained all treatment conditions. After four to five weeks (for iT<sub>reg</sub> cell comparisons) or eight weeks (for the transgenic T cell comparisons), large intestines were collected and fixed with 10% neutral buffered formalin (Fisher). Samples were sectioned and stained with haematoxylin and eosin (H&E) by the Histopathology Core at the New York University School of Medicine.

**Histology analysis.** The H&E slides from each sample were examined in a blinded fashion. Samples of proximal, mid and distal colon were graded semi-quantitatively from 0 to 4 as described previously<sup>39</sup>. Scores from proximal, mid and distal sites were averaged to obtain inflammation scores for the entire colon.

**Cell isolation for RNA-seq experiment.** A T cell reconstitution system was designed to purify c-MAF-sufficient or -deficient iT<sub>reg</sub> cells from compatible microenvironments. In brief,  $T_{naive}$  cells were isolated from the spleen of CD45.2 *Foxp3*<sup>creYFP</sup> or *Maf*<sup>ΔTreg</sup> mice as CD4<sup>+</sup>CD3<sup>+</sup>CD44<sup>lo</sup>CD62L<sup>hi</sup>FOXP3-YFP and iT<sub>reg</sub> cells were isolated from the spleens of CD45.1 wild-type B6 mice as CD4<sup>+</sup>CD3<sup>+</sup>CD25<sup>+</sup> by FACS.  $T_{naive}$  cells ( $2 \times 10^5$ ) and iT<sub>reg</sub> cells ( $8 \times 10^5$ ) were simultaneously administered by retro-orbital injection into *H. hepaticus*-colonized *Rag1*<sup>-/-</sup> mice. Two weeks after transfer, c-MAF-sufficient or -deficient iT<sub>reg</sub> cells were purified from the large intestine of reconstituted mice as CD4<sup>+</sup>CD3<sup>+</sup>CD45.1<sup>-</sup>CD45.2<sup>+</sup>FOXP3-YFP<sup>+</sup> by FACS and collected into FBS. 20% of the sorted cells were stained for RORγt and FOXP3 and the remaining cells were saved in TRIzol (Invitrogen) for RNA extraction.

To isolate *H. hepaticus*-specific colitogenic T<sub>eff</sub> cells, HH7-2tg; *Maf*<sup>ΔTreg</sup> and HH7-2tg; *Foxp3*<sup>cre</sup> mice were colonized with *H. hepaticus*. HH7-2tg; *Foxp3*<sup>cre</sup> mice were further injected intraperitoneally with 1 mg anti-IL-10RA antibody (clone 1B1.3A, Bioxcell) weekly from the day of colonization. HH7-2 T<sub>eff</sub> cells (CD3<sup>+</sup>CD4<sup>+</sup>TCRV36<sup>+</sup>FOXP3<sup>-</sup>YFP<sup>-</sup>) were sorted from the LILP two weeks after colonization. Homeostatic IL-23R-GFP<sup>+</sup> T cells (CD3<sup>+</sup>CD4<sup>+</sup>IL-23R-GFP<sup>+</sup>) were sorted from both SILP and LILP of *Il23r*<sup>GFP/+</sup> mice stably colonized with SFB.

**RNA-seq library preparation.** Total RNA was extracted using TRIzol (Invitrogen) followed by DNase I treatment and cleanup with RNeasy MinElute kit (Qiagen). iT<sub>reg</sub> cell RNA-seq libraries were prepared with the SMART-Seq v4 Ultra Low Input RNA Kit (Clontech 634899 and 634888). T<sub>17</sub> cell RNA libraries were prepared using the Nugen Ovation Ultralow Library Systems V2 (7102 and 0344). All sequencing was performed using the Illumina NextSeq. RNA-seq libraries were prepared and sequenced by the Genome Technology Core at New York University School of Medicine.

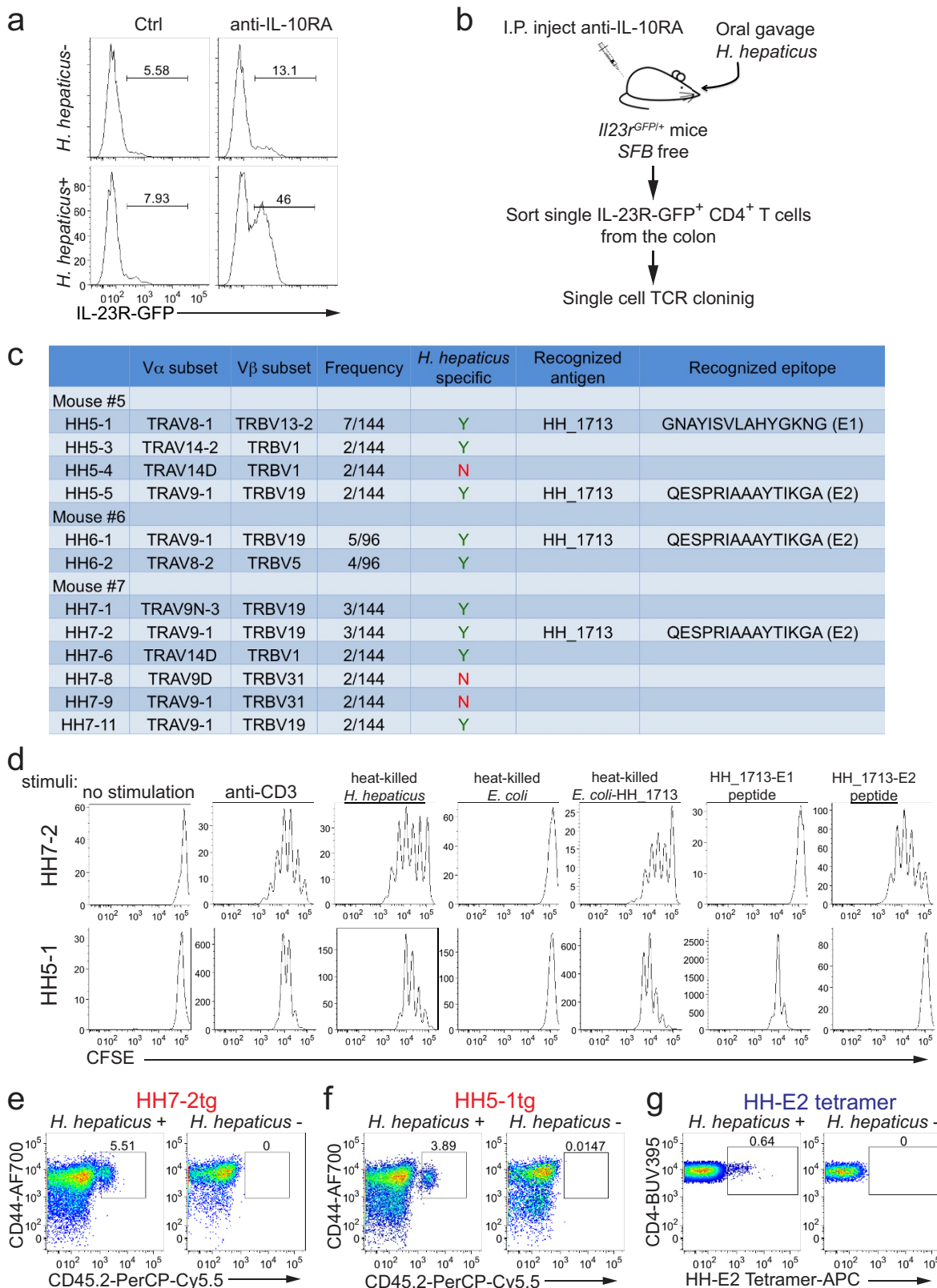
**Data processing of RNA-seq.** RNA-seq reads were mapped to the *Mus musculus* genome Ensembl annotation release 87 with STAR (v2.5.2b)<sup>40</sup>. Uniquely mapped reads were counted using featureCounts<sup>41</sup> with parameters: -p -Q 20. DESeq2<sup>42</sup> was used to identify differentially expressed genes across conditions with experimental design: ~condition + gender. Read counts were normalized and transformed by functions varianceStabilizingTransformation and rlog in DESeq2 with the following parameter: blind=FALSE. Gender differences were considered as batch effect, and were corrected by ComBat<sup>43</sup>. Downstream analysis and data visualization were performed in R<sup>44</sup>.

**Statistical analysis.** For animal studies, mutant and control groups did not always have similar standard deviations and therefore an unpaired two-sided Welch's t-test was used. Error bars represent  $\pm$  s.d. Animal sample size estimates were determined using power analysis (power = 90% and  $\alpha = 0.05$ ) based on the mean and s.d.

from our previous studies and/or pilot studies using 4–5 mice. No samples were excluded from analysis. For RNA-seq analysis, differentially expressed genes were calculated in DESeq2 using the Wald test with Benjamini–Hochberg correction to determine the FDR. Genes were considered differentially expressed with FDR < 0.1 and log<sub>2</sub> fold change > 1.5. Enriched disease pathways in pathogenic HH7-2 T<sub>H</sub>17 were determined using Ingenuity Pathway Analysis (<https://www.ingenuity.com>). Gene set enrichment analysis (GSEA, <http://www.broad.mit.edu/gsea/>) on *Maf*-deficient or -sufficient iT<sub>reg</sub> cells was performed using a gene set of 33 ROR $\gamma$ t-dependent genes in NRPI<sup>−</sup> colonic T<sub>reg</sub> cells (*Rorc*, *Ccr6*, *Idua*, *Il1rn*, *C2cd4b*, *Nxt1*, *Tmem176b*, *Cxcr3*, *Tnfrsf1a*, *Adams7*, *Pik3ip1*, *Rrad*, *Crrmp1*, *Irak3*, *Fam129b*, *Ppc5*, *Tbx2a2r*, *Avp1*, *Serpina1a*, *Alkbh7*, *Nckipsd*, *Havcr2*, *Il23r*, *Txnip*, *Igj* (also known as *Jchain*), *Trim16*, *Pigr*, *Rras*, *Samd10*, *Il1r2*, *F2rl1*, *Maff* and *Ly6c1*)<sup>11</sup>.

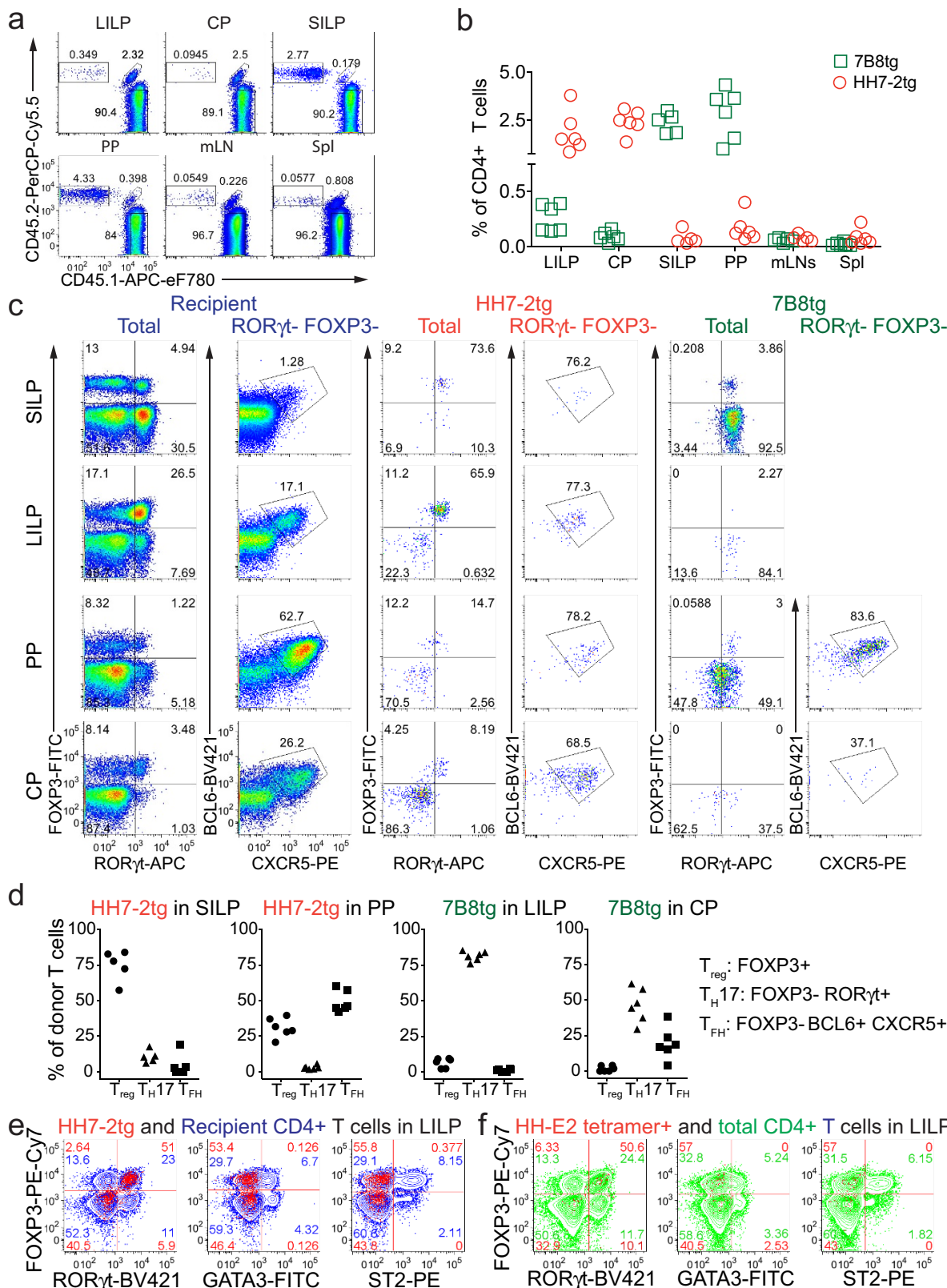
**Data availability.** cDNA sequences of *H. hepaticus*-specific TCRs yielding data that support the findings of this study have been deposited in GenBank with the accession codes KY964547–KY964570. RNA-seq data have been deposited in the Sequence Read Archive (SRA) with accession code SRP126932, and in the Gene Expression Omnibus (GEO) with accession code GSE108184. All other data are available from the corresponding author upon reasonable request.

28. Rubtsov, Y. P. *et al.* Regulatory T cell-derived interleukin-10 limits inflammation at environmental interfaces. *Immunity* **28**, 546–558 (2008).
29. Wende, H. *et al.* The transcription factor c-Maf controls touch receptor development and function. *Science* **335**, 1373–1376 (2012).
30. Awasthi, A. *et al.* Cutting edge: IL-23 receptor GFP reporter mice reveal distinct populations of IL-17-producing cells. *J. Immunol.* **182**, 5904–5908 (2009).
31. Dash, P. *et al.* Paired analysis of TCR $\alpha$  and TCR $\beta$  chains at the single-cell level in mice. *J. Clin. Invest.* **121**, 288–295 (2011).
32. Lefranc, M. P. *et al.* IMGT, the international ImMunoGeneTics information system. *Nucleic Acids Res.* **37**, D1006–D1012 (2009).
33. Ise, W. *et al.* CTLA-4 suppresses the pathogenicity of self antigen-specific T cells by cell-intrinsic and cell-extrinsic mechanisms. *Nat. Immunol.* **11**, 129–135 (2010).
34. Mach, N. *et al.* Differences in dendritic cells stimulated in vivo by tumors engineered to secrete granulocyte-macrophage colony-stimulating factor or Flt3-ligand. *Cancer Res.* **60**, 3239–3246 (2000).
35. Reche, P. A. & Reinherz, E. L. Prediction of peptide–MHC binding using profiles. *Methods Mol. Biol.* **409**, 185–200 (2007).
36. Kouskoff, V., Signorelli, K., Benoist, C. & Mathis, D. Cassette vectors directing expression of T cell receptor genes in transgenic mice. *J. Immunol. Methods* **180**, 273–280 (1995).
37. Altman, J. D. *et al.* Phenotypic analysis of antigen-specific T lymphocytes. *Science* **274**, 94–96 (1996).
38. Ostianin, D. V. *et al.* T cell transfer model of chronic colitis: concepts, considerations, and tricks of the trade. *Am. J. Physiol. Gastrointest. Liver Physiol.* **296**, G135–G146 (2009).
39. Read, S., Malmström, V. & Powrie, F. Cytotoxic T lymphocyte-associated antigen 4 plays an essential role in the function of CD25<sup>+</sup>CD4<sup>+</sup> regulatory cells that control intestinal inflammation. *J. Exp. Med.* **192**, 295–302 (2000).
40. Dobin, A. *et al.* STAR: ultrafast universal RNA-seq aligner. *Bioinformatics* **29**, 15–21 (2013).
41. Liao, Y., Smyth, G. K. & Shi, W. featureCounts: an efficient general purpose program for assigning sequence reads to genomic features. *Bioinformatics* **30**, 923–930 (2014).
42. Love, M. I., Huber, W. & Anders, S. Moderated estimation of fold change and dispersion for RNA-seq data with DESeq2. *Genome Biol.* **15**, 550 (2014).
43. Johnson, W. E., Li, C. & Rabinovic, A. Adjusting batch effects in microarray expression data using empirical Bayes methods. *Biostatistics* **8**, 118–127 (2007).
44. R Development Core Team. *R: A Language And Environment For Statistical Computing*; <https://www.r-project.org/> (R Foundation for Statistical Computing, Vienna, Austria, 2016).



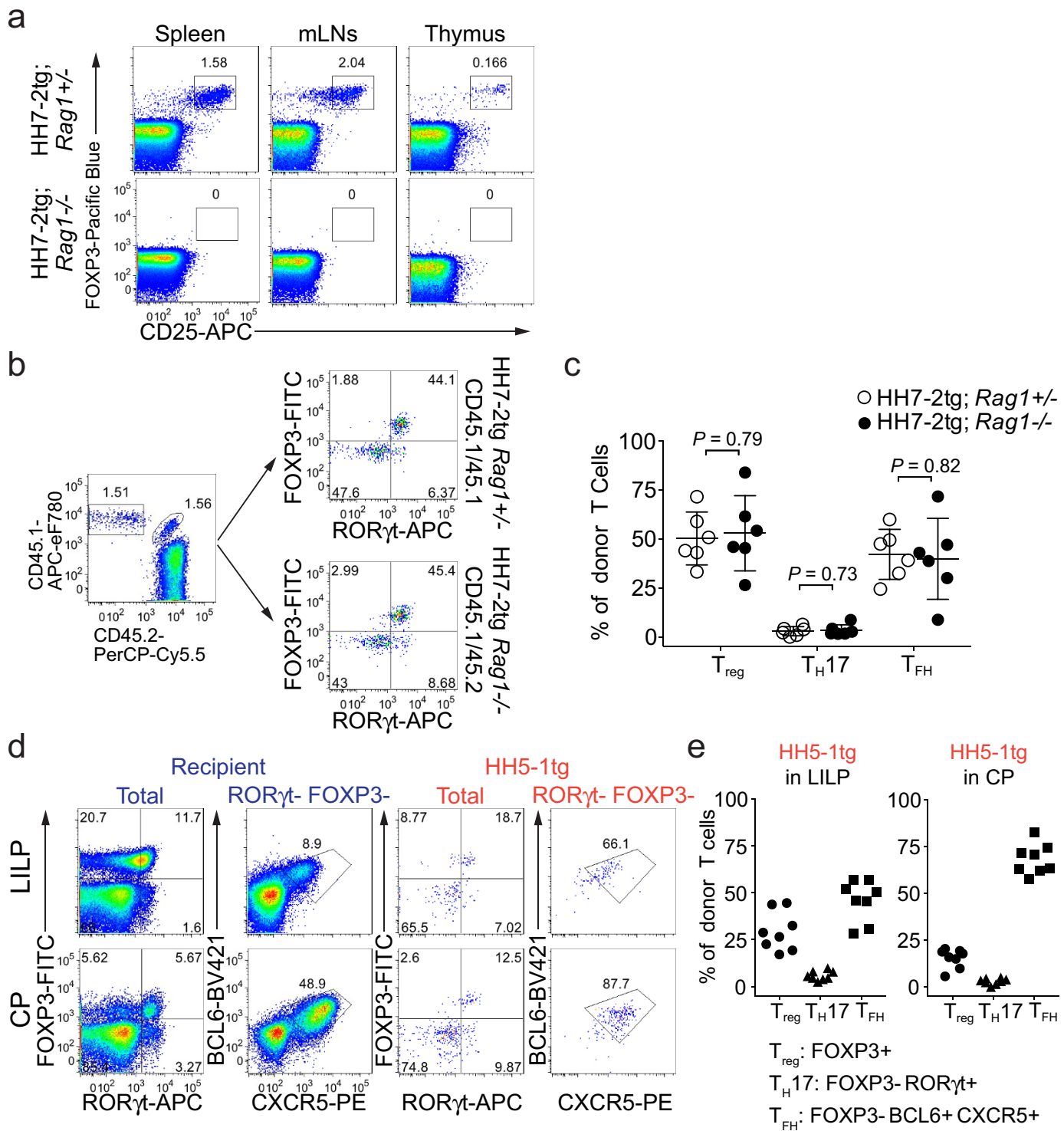
**Extended Data Figure 1 | Cloning and characterization of *H. hepaticus*-specific T<sub>H</sub>17 TCRs, and generation of TCRtg mice and MHC class II tetramers.** **a**, IL-23R-GFP expression in CD4<sup>+</sup> T cells from the large intestines of mice with and without *H. hepaticus* colonization and after IL-10RA blockade. Data are from one of five independent experiments. **b**, Experimental scheme for cloning *H. hepaticus*-induced single IL-23R-GFP<sup>+</sup> (predominantly T<sub>H</sub>17) cell TCRs under IL-10RA blockade. **c**, Summary of the 12 dominant *H. hepaticus*-induced T<sub>H</sub>17 TCRs.

**d**, In vitro activation of CFSE-labelled naive HH7-2tg and HH5-1tg cells by indicated stimuli in the presence of antigen-presenting cells. Data are from one of two independent experiments. **e**, **f**, Expansion of donor-derived HH7-2tg (**e**) and HH5-1tg (**f**) (CD45.2) cells in the large intestine of *H. hepaticus*-colonized or -free CD45.1 mice, gated on total CD4<sup>+</sup> T cells. Data are from one of three independent experiments. **g**, HH-E2 tetramer staining of CD4<sup>+</sup> T cells from the large intestine of *H. hepaticus*-colonized or -free mice. Data are from one of six independent experiments.



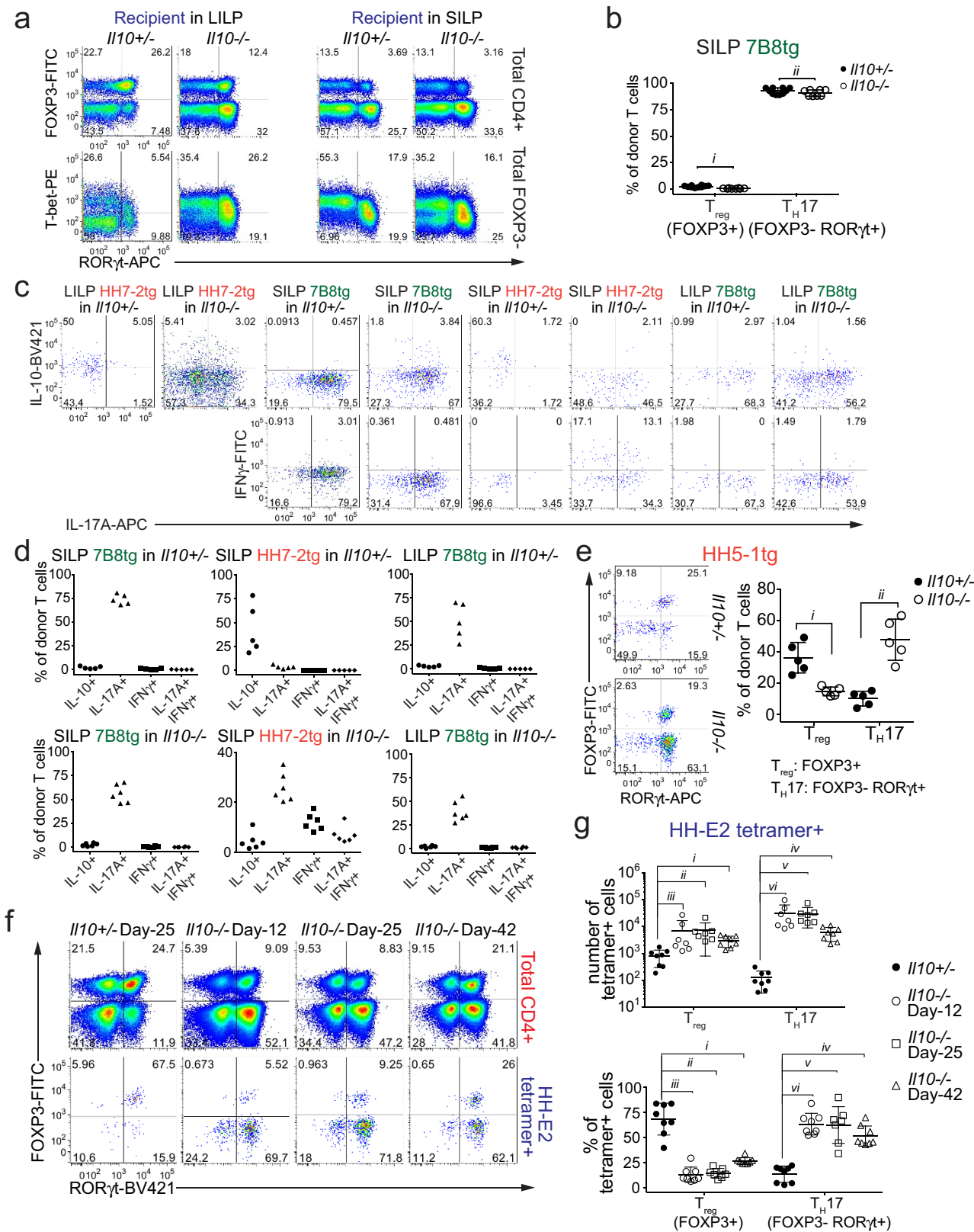
**Extended Data Figure 2 | Extended characterization of SFB- and *H. hepaticus*-specific T cells in distinct anatomical sites in bacteria-colonized wild-type mice.** **a**, Representative flow cytometry plots of donor-derived HH7-2tg (CD45.1/45.2) and 7B8tg (CD45.2/45.2) T cells in indicated tissues of mice colonized with SFB and *H. hepaticus*, gated on total CD4<sup>+</sup> T cells (CD4<sup>+</sup>CD3<sup>+</sup>) ( $n=15$ ). **b**, Proportions of donor-derived HH7-2tg and 7B8tg T cells among total CD4<sup>+</sup> T cells in indicated tissues. Data in **a** and **b** are from 1 of 3 experiments, with a total of 15 mice in the 3 experiments. **c**, Representative flow cytometry plots of ROR $\gamma$ t, FOXP3, BCL6 and CXCR5 expression in CD4<sup>+</sup> T cells from the host and from

HH7-2tg and 7B8tg donors in different tissues ( $n=15$ ). **d**, Frequencies of T<sub>reg</sub> (FOXP3<sup>+</sup>), T<sub>H</sub>17 (FOXP3<sup>-</sup>ROR $\gamma$ t<sup>+</sup>) and T<sub>FH</sub> (BCL6<sup>+</sup>CXCR5<sup>+</sup>) cells among donor-derived HH7-2tg and 7B8tg cells in different tissues. Data are from 1 of 3 experiments, with a total of 15 mice in the 3 experiments. **e**, Representative flow cytometry plots of FOXP3, ROR $\gamma$ t, GATA3 and ST2 expression in CD4<sup>+</sup> T cells from the host (blue) and from HH7-2tg donors (red) in the LILP ( $n=5$ ). **f**, Representative flow cytometry plots of FOXP3, ROR $\gamma$ t, GATA3 and ST2 expression in total CD4<sup>+</sup> (green) and HH-E2 tetramer<sup>+</sup> (red) T cells in the LILP ( $n=5$ ). Spl, spleen.



**Extended Data Figure 3 | Extended characterization of *H. hepaticus*-specific TCRtg cell differentiation.** **a**, HH7-2tg; *Rag1*<sup>−/−</sup> mice do not develop T<sub>reg</sub> cells in the thymus. Representative flow cytometry plots of T<sub>reg</sub> (FOXP3<sup>+</sup>CD25<sup>+</sup>) frequency in indicated tissues of *H. hepaticus*-free HH7-2tg; *Rag1*<sup>+/−</sup> ( $n=3$ ) or HH7-2tg; *Rag1*<sup>−/−</sup> ( $n=3$ ) mice. **b, c**, HH7-2tg; *Rag1*<sup>−/−</sup> and HH7-2tg; *Rag1*<sup>+/−</sup> donor-derived T cells differentiated into equal frequencies of ROR $\gamma$ t<sup>+</sup> T<sub>reg</sub> cells in the large intestine of wild-type mice. Equal numbers (2,000) of congenic isotype-labelled HH7-2tg; *Rag1*<sup>+/−</sup> (CD45.1/45.1) and *Rag1*<sup>−/−</sup> (CD45.1/45.2) naive T cells were co-transferred into *H. hepaticus*-colonized wild-type B6 mice. Cells from the LILP were analysed two weeks after transfer. Data summarize two independent experiments ( $n=6$ ). **b**, Representative flow cytometry plots of donor and recipient T cell frequency (left), and ROR $\gamma$ t and FOXP3 expression (right) ( $n=6$ ). **c**, Frequencies of T<sub>reg</sub>

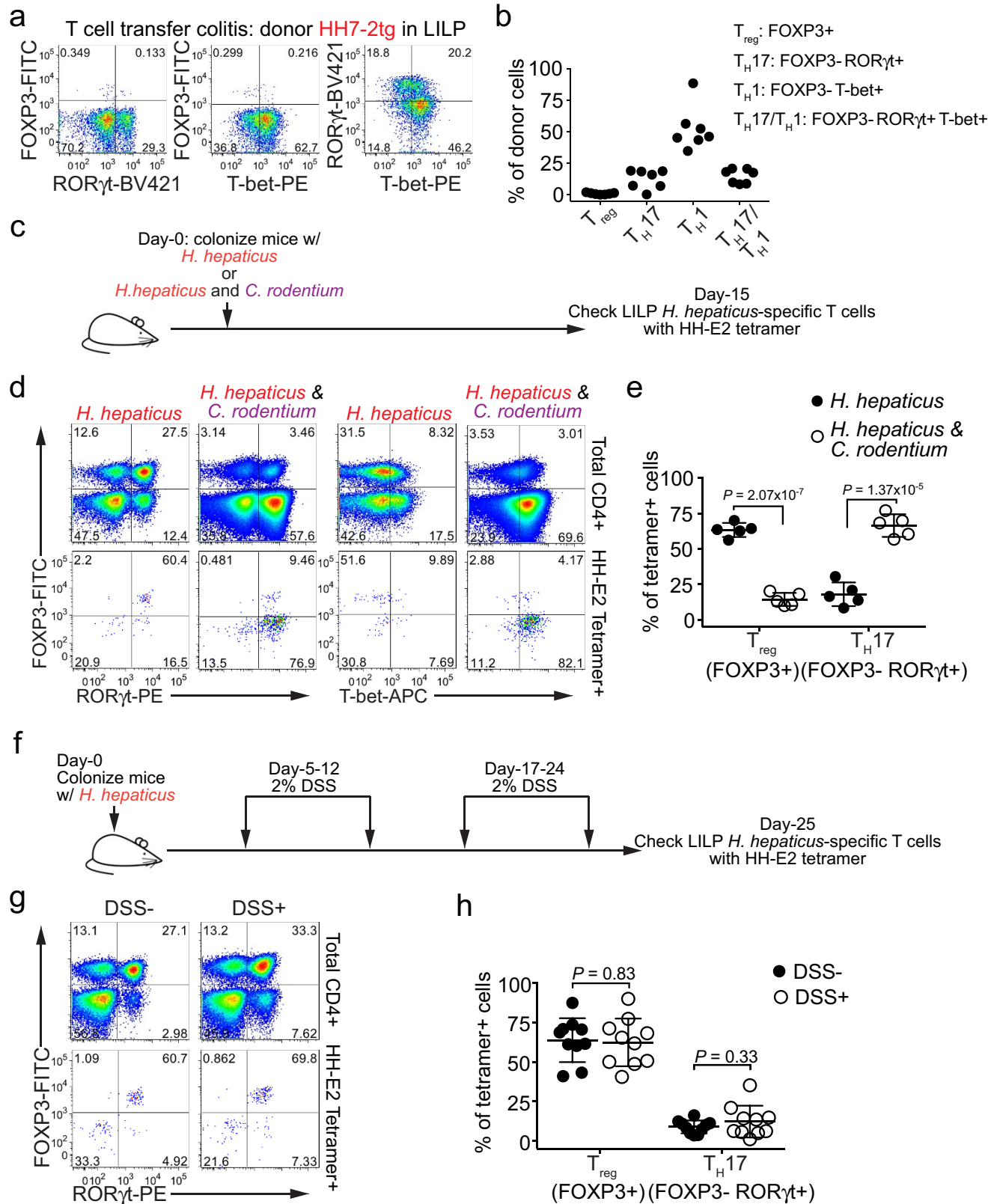
(FOXP3<sup>+</sup>), T<sub>H</sub>17 (FOXP3<sup>−</sup>ROR $\gamma$ t<sup>+</sup>) and T<sub>FH</sub> (BCL6<sup>+</sup>CXCR5<sup>+</sup>) cells among HH7-2tg *Rag1*<sup>+/−</sup> ( $n=6$ ) and *Rag1*<sup>−/−</sup> ( $n=6$ ) donor-derived T cells. **d, e**, Approximately 2,000 naive HH5-1tg cells (CD45.1/45.2) were adoptively transferred into wild-type B6 mice (CD45.2/45.2) colonized with *H. hepaticus*. Cells from LILP and the caecal patch were analysed two weeks after transfer. **d**, Representative flow cytometry plots are shown for ROR $\gamma$ t, FOXP3, BCL6 and CXCR5 expression in donor-derived and recipient CD4<sup>+</sup> T cells in the indicated tissues. **e**, Frequencies of T<sub>reg</sub> (FOXP3<sup>+</sup>), T<sub>H</sub>17 (FOXP3<sup>−</sup>ROR $\gamma$ t<sup>+</sup>) and T<sub>FH</sub> (BCL6<sup>+</sup>CXCR5<sup>+</sup>) among HH5-1tg donor T cells ( $n=8$ ). Data are a summary of eight mice from two independent experiments. All statistics were calculated by unpaired two-sided Welch's *t*-test. Error bars denote mean  $\pm$  s.d. *P* values are indicated on the figure.



Extended Data Figure 4 | See next page for caption.

**Extended Data Figure 4 | Differentiation of SFB- and *H. hepaticus*-specific T cells in *Il10<sup>+/−</sup>* and *Il10<sup>−/−</sup>* mice.** **a–d**, Equal numbers (10,000) of congenic isotype-labelled HH7-2tg (CD45.1/45.2) and 7B8tg (CD45.2/45.1) T cells were co-transferred into *Il10<sup>−/−</sup>* and *Il10<sup>+/−</sup>* mice colonized with both *H. hepaticus* and SFB. Intestinal T cells were examined two weeks later. **a**, Representative flow cytometry plots of FOXP3, ROR $\gamma$ t and T-bet expression in total and FOXP3 $^{−}$  host CD4 $^{+}$  T cells in the SILP and LILP of *Il10<sup>+/−</sup>* ( $n = 10$ ) and *Il10<sup>−/−</sup>* ( $n = 8$ ) mice that received TCR transgenic T cell transplants. **b**, Frequencies of T $_{\text{reg}}$  (FOXP3 $^{+}$ ) and T $_{\text{H}17}$  (FOXP3 $^{-}$ ROR $\gamma$ t $^{+}$ ) cells among SILP 7B8tg donor-derived cells in *Il10<sup>+/−</sup>* ( $n = 10$ ) and *Il10<sup>−/−</sup>* ( $n = 8$ ) mice. Data for **a** and **b** are a summary of four independent experiments. **c**, Representative flow cytometry plots of IL-10, IL-17A and IFN $\gamma$  expression in transferred 7B8tg and HH7-2tg cells from LILP and SILP of *Il10<sup>+/−</sup>* and *Il10<sup>−/−</sup>* mice after re-stimulation ( $n = 5$  or 6). **d**, Proportions of transferred 7B8tg and HH7-2tg cells in the SILP and LILP of *Il10<sup>+/−</sup>* and *Il10<sup>−/−</sup>* mice that express IL-10, IL-17A and IFN $\gamma$  after re-stimulation ( $n = 5$  or 6). Data for

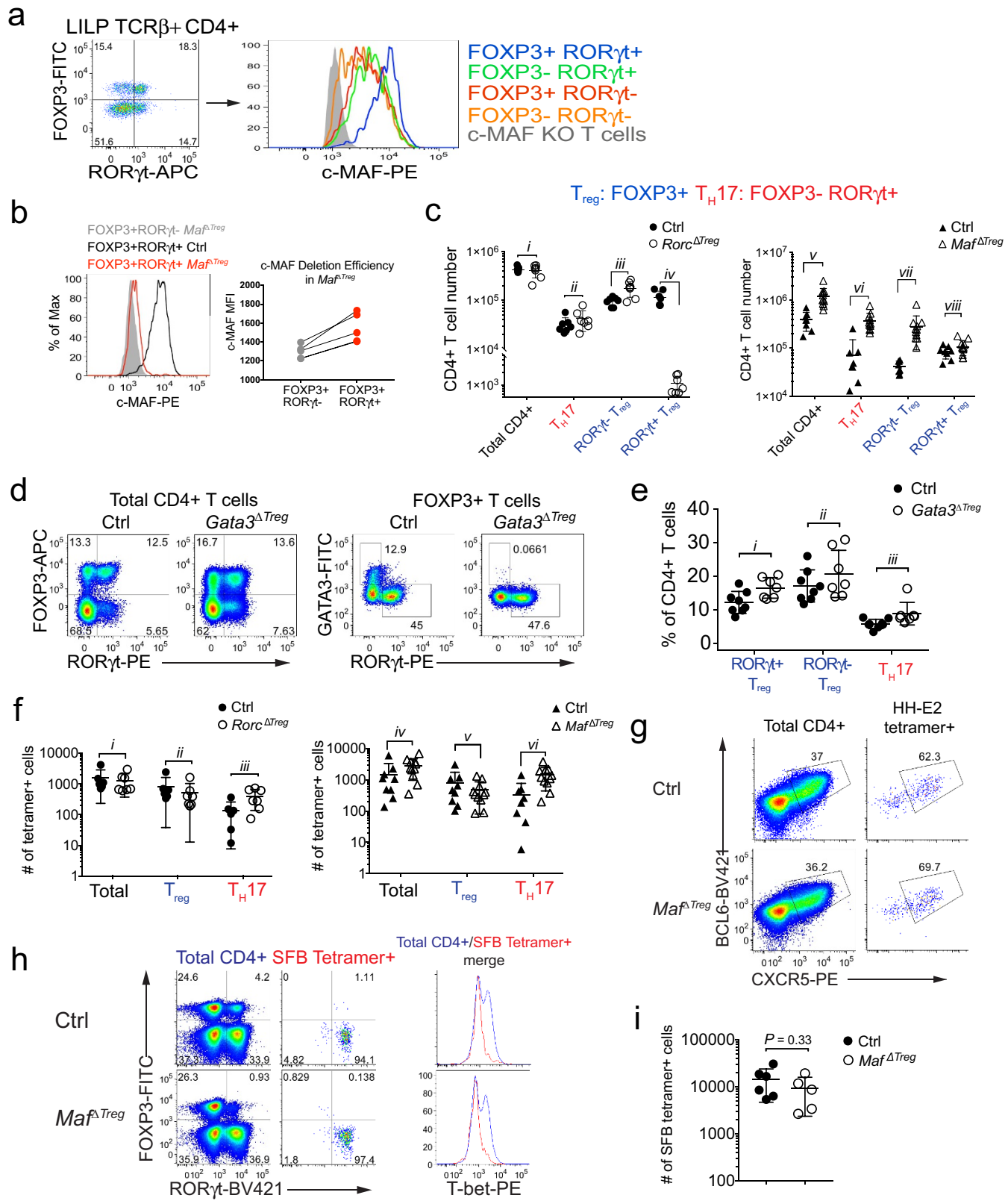
**c** and **d** are a summary of two independent experiments. **e**, 2,000 naive HH5-1tg cells (CD45.1/45.2) were adoptively transferred into *Il10<sup>+/−</sup>* and *Il10<sup>−/−</sup>* mice colonized with *H. hepaticus*. Cells from the LILP were analysed two weeks after transfer ( $n = 5$ ). Representative flow cytometry plots of ROR $\gamma$ t and FOXP3 expression in HH5-1tg donor cells are shown (left), along with a compilation of frequencies of T $_{\text{reg}}$  (FOXP3 $^{+}$ ) and T $_{\text{H}17}$  (FOXP3 $^{-}$ ROR $\gamma$ t $^{+}$ ). **f**, **g**, ROR $\gamma$ t and FOXP3 expression in total CD4 $^{+}$  and HH-E2 tetramer $^{+}$  T cells (**f**) and frequencies (above) and absolute numbers (below) of T $_{\text{reg}}$  (FOXP3 $^{+}$ ) and T $_{\text{H}17}$  (FOXP3 $^{-}$ ROR $\gamma$ t $^{+}$ ) cells among HH-E2 tetramer $^{+}$  T cells (**g**) in the LILP of *Il10<sup>+/−</sup>* (day 25,  $n = 8$ ) and *Il10<sup>−/−</sup>* (day 12  $n = 8$ , day 25  $n = 7$ , day 42  $n = 8$ ) mice colonized with *H. hepaticus* for indicated times. All statistics were calculated by unpaired two-sided Welch's *t*-test. Error bars denote mean  $\pm$  s.d. *P* values are as follows: **b**, i = 0.062 and ii = 0.063. **e**, i =  $1.46 \times 10^{-3}$  and ii =  $3.10 \times 10^{-4}$ . **g**, Top, i =  $7.82 \times 10^{-4}$ , ii = 0.014, iii = 0.088, iv =  $1.48 \times 10^{-4}$ , v =  $1.47 \times 10^{-3}$  and vi = 0.016; bottom, i =  $3.85 \times 10^{-6}$ , ii =  $9.63 \times 10^{-7}$ , iii =  $1.31 \times 10^{-6}$ , iv =  $8.91 \times 10^{-7}$ , v =  $1.15 \times 10^{-5}$  and vi =  $1.56 \times 10^{-7}$ .



Extended Data Figure 5 | See next page for caption.

**Extended Data Figure 5 | Differentiation of *H. hepaticus*-specific T cells in colitis models.** **a, b**, Naive HH7-2tg T cells were adoptively transferred into *H. hepaticus*-colonized *Rag1*<sup>−/−</sup> mice to induce colitis ( $n = 7$ ). Data summarize two independent experiments. Representative expression of FOXP3, ROR $\gamma$ t, and T-bet (**a**), and a compilation of frequencies of T<sub>reg</sub> (FOXP3 $^{+}$ ), T<sub>H</sub>17 (FOXP3 $^{-}$ ROR $\gamma$ t $^{+}$ ), T<sub>H</sub>1 (FOXP3 $^{-}$ T-bet $^{+}$ ) and T<sub>H</sub>17/T<sub>H</sub>1 (FOXP3 $^{-}$ ROR $\gamma$ t $^{+}$ T-bet $^{+}$ ) cells in HH7-2tg donor-derived cells in the LILP of recipient mice was analysed 4 weeks after transfer. **c–e**, Analysis of *H. hepaticus*-specific T cell differentiation during *C. rodentium*-induced colonic inflammation. Data summarize two independent experiments. **c**, Schematic of experimental design. **d, e**, Representative flow cytometry plots of FOXP3, ROR $\gamma$ t and T-bet expression in total CD4 $^{+}$  and HH-E2

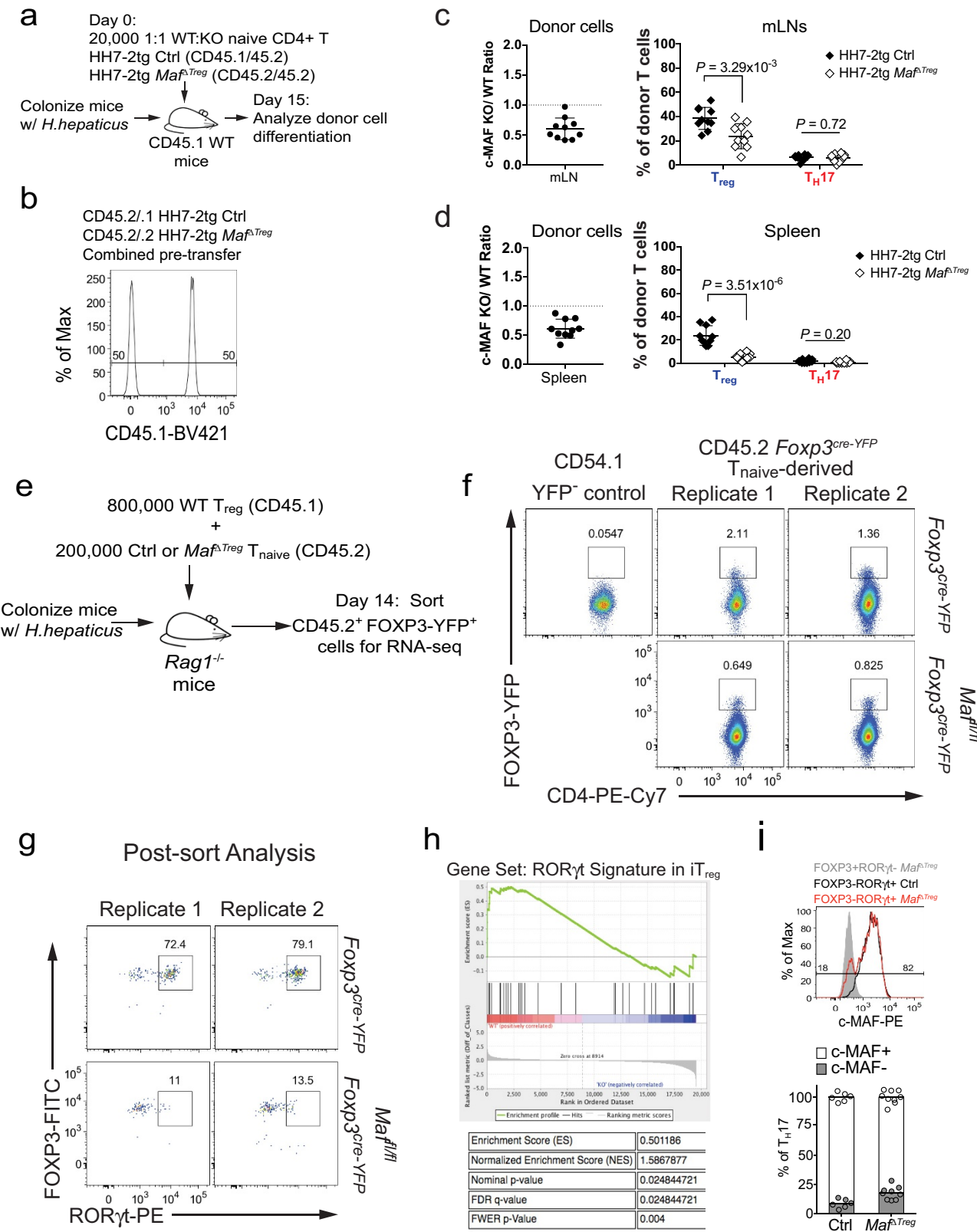
tetramer $^{+}$  T cells (**d**) and frequencies of T<sub>reg</sub> (FOXP3 $^{+}$ ) and T<sub>H</sub>17 (FOXP3 $^{-}$ ROR $\gamma$ t $^{+}$ ) cells among HH-E2 tetramer $^{+}$  T cells (**e**) in the LILP of *C. rodentium*-infected ( $n = 5$ ) and -uninfected mice ( $n = 5$ ). **f–h**, Analysis of *H. hepaticus*-specific T cell differentiation during DSS-induced colitis. Data are a summary of two independent experiments. **f**, Schematic of experimental design. **g, h**, Representative flow cytometry plots of FOXP3, ROR $\gamma$ t and T-bet expression in total CD4 $^{+}$  and HH-E2 tetramer $^{+}$  T cells (**g**) and a compilation of frequencies of T<sub>reg</sub> (FOXP3 $^{+}$ ) and T<sub>H</sub>17 (FOXP3 $^{-}$ ROR $\gamma$ t $^{+}$ ) cells among HH-E2 tetramer $^{+}$  cells (**h**) in the LILP of DSS-treated ( $n = 10$ ) and -untreated mice ( $n = 10$ ). All statistics were calculated by unpaired two-sided Welch's *t*-test. Error bars denote mean  $\pm$  s.d. *P* values are indicated on the figure.



Extended Data Figure 6 | See next page for caption.

**Extended Data Figure 6 | Extended characterization of *Maf*<sup>ΔTreg</sup>, *Rorc*<sup>ΔTreg</sup> and *Gata3*<sup>ΔTreg</sup> mice.** **a**, Expression of c-MAF in the indicated CD4<sup>+</sup> T cell subsets in the LILP. **b**, Incomplete depletion of c-MAF protein in ROR $\gamma$ t<sup>+</sup> T<sub>reg</sub> cells in *Maf*<sup>ΔTreg</sup> mice shown by a representative flow cytometry graph from 3 independent experiments (left), and a compilation of mean fluorescence intensities (MFI) in ROR $\gamma$ t<sup>−</sup> T<sub>reg</sub> cells and residual ROR $\gamma$ t<sup>+</sup> T<sub>reg</sub> cells (right). **c**, Absolute numbers of indicated CD4<sup>+</sup> T cell populations in the LILP of indicated mice. Data are a summary of 3 independent experiments for *Rorc*<sup>ΔTreg</sup> ( $n=7$ ) and littermate controls ( $n=7$ ) and 4 independent experiments for *Maf*<sup>ΔTreg</sup> ( $n=11$ ) and littermate controls ( $n=8$ ). **d, e**, Representative flow cytometry plots of FOXP3, ROR $\gamma$ t and GATA3 expression in total and FOXP3<sup>+</sup> CD4<sup>+</sup> T cells (**d**) and a compilation of frequencies of ROR $\gamma$ t<sup>+</sup> and ROR $\gamma$ t<sup>−</sup> T<sub>reg</sub> (FOXP3<sup>+</sup>) cells and T<sub>H</sub>17 (FOXP3<sup>−</sup> ROR $\gamma$ t<sup>+</sup>) cells among total CD4<sup>+</sup> T cells (**e**) in the LILP of *Gata3*<sup>ΔTreg</sup> ( $n=8$ ) and littermate controls ( $n=7$ ). Data summarize two independent experiments. **f**, Absolute numbers of indicated HH-E2 tetramer<sup>+</sup> T cell populations in the LILP of indicated

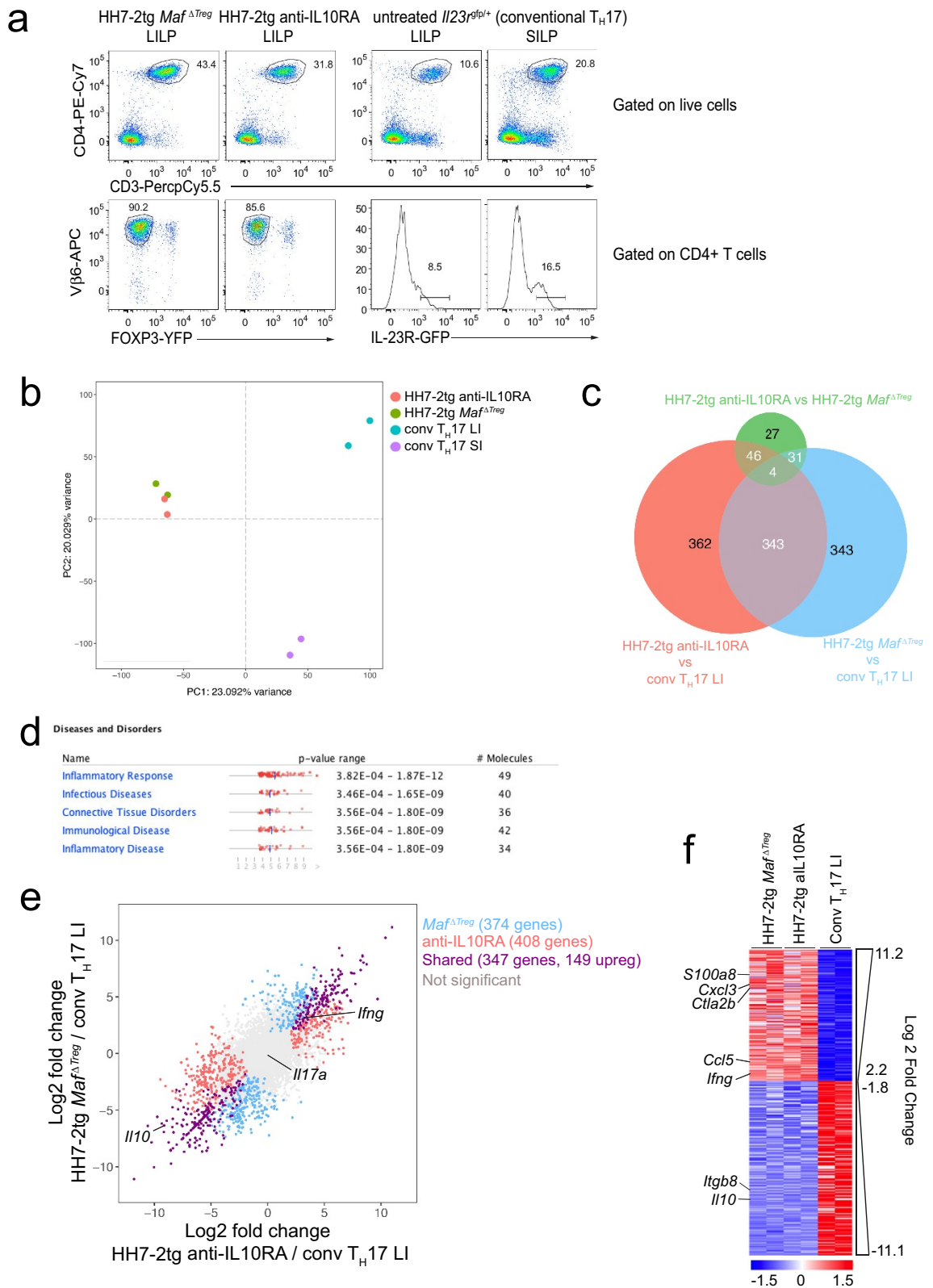
mice. Data are a summary of 3 independent experiments for *Rorc*<sup>ΔTreg</sup> ( $n=7$ ) and littermate controls ( $n=6$ ) and 4 independent experiments for *Maf*<sup>ΔTreg</sup> ( $n=11$ ) and littermate controls ( $n=8$ ). **g**, Representative flow cytometry plots of T<sub>FH</sub> markers BCL6 and CXCR5 among total CD4<sup>+</sup> and HH-E2 tetramer<sup>+</sup> cells from the caecal patch of *Maf*<sup>ΔTreg</sup> mice and littermate controls ( $n=4$ ). **h, i**, SFB-specific T cells did not adopt the pro-inflammatory T<sub>H</sub>17-T<sub>H</sub>1 phenotype or expand in *Maf*<sup>ΔTreg</sup> mice. Data summarize two experiments, *Maf*<sup>ΔTreg</sup> ( $n=5$ ) and littermate controls ( $n=6$ ). Representative flow cytometry plots of FOXP3, ROR $\gamma$ t and T-bet expression in total CD4<sup>+</sup> and SFB-tetramer<sup>+</sup> T cells (**h**) and absolute number of SFB-tetramer<sup>+</sup> cells (**i**) in the SILP. All statistics were calculated by unpaired two-sided Welch's *t*-test. Error bars denote mean  $\pm$  s.d. *P* values are indicated on the figure or as follows: **c**, *i* = 0.42, *ii* = 0.73, *iii* =  $6.38 \times 10^{-3}$ , *iv* =  $2.28 \times 10^{-4}$ , *v* =  $7 \times 10^{-11}$ , *vi* =  $7.10 \times 10^{-3}$ , *vii* =  $2.99 \times 10^{-2}$  and *viii* = 0.83. **e**, *i* = 0.081, *ii* = 0.102 and *iii* = 0.16. **f**, *i* = 0.65, *ii* = 0.41, *iii* = 0.045, *iv* = 0.12, *v* = 0.29 and *vi* =  $6.28 \times 10^{-3}$ .



Extended Data Figure 7 | See next page for caption.

**Extended Data Figure 7 | Analysis of c-MAF function in ROR $\gamma$ t<sup>+</sup> iT<sub>reg</sub> cells.** **a–d**, Equal numbers of congenic isotype-labelled naïve *Maf*<sup>fl/fl</sup>; *Foxp3*<sup>cre</sup> (ctrl, CD45.1/45.2) and *Maf*<sup>Δ/Δ</sup>; *Foxp3*<sup>cre</sup> (CD45.2/45.2) HH7-2tg cells were co-transferred into *H. hepaticus*-colonized wild-type CD45.1 mice. Cells from the LILP, mLNs and spleen were analysed 15 days after transfer. **a**, Schematic of experimental design. **b**, Flow cytometry plot depicting ratio of pooled co-transferred naïve T cells before transfer. **c, d**, Left, ratios of *Maf*<sup>Δ/Δ</sup> versus control HH7-2tg donor-derived cells in the mLNs and spleen ( $n = 10$ ). Dashed line represents ratio of co-transferred cells before transfer. Right, frequencies of T<sub>reg</sub> (FOXP3<sup>+</sup>) and T<sub>H</sub>17 (FOXP3<sup>−</sup>ROR $\gamma$ t<sup>+</sup>) cells among donor-derived cells ( $n = 10$ ). Statistics were calculated by unpaired two-sided Welch's *t*-test. Error bars denote mean  $\pm$  s.d. *P* values are indicated on the figure. **e–h**, Isolation of *Maf*-deficient and -sufficient iT<sub>reg</sub> cells for RNA-seq through a

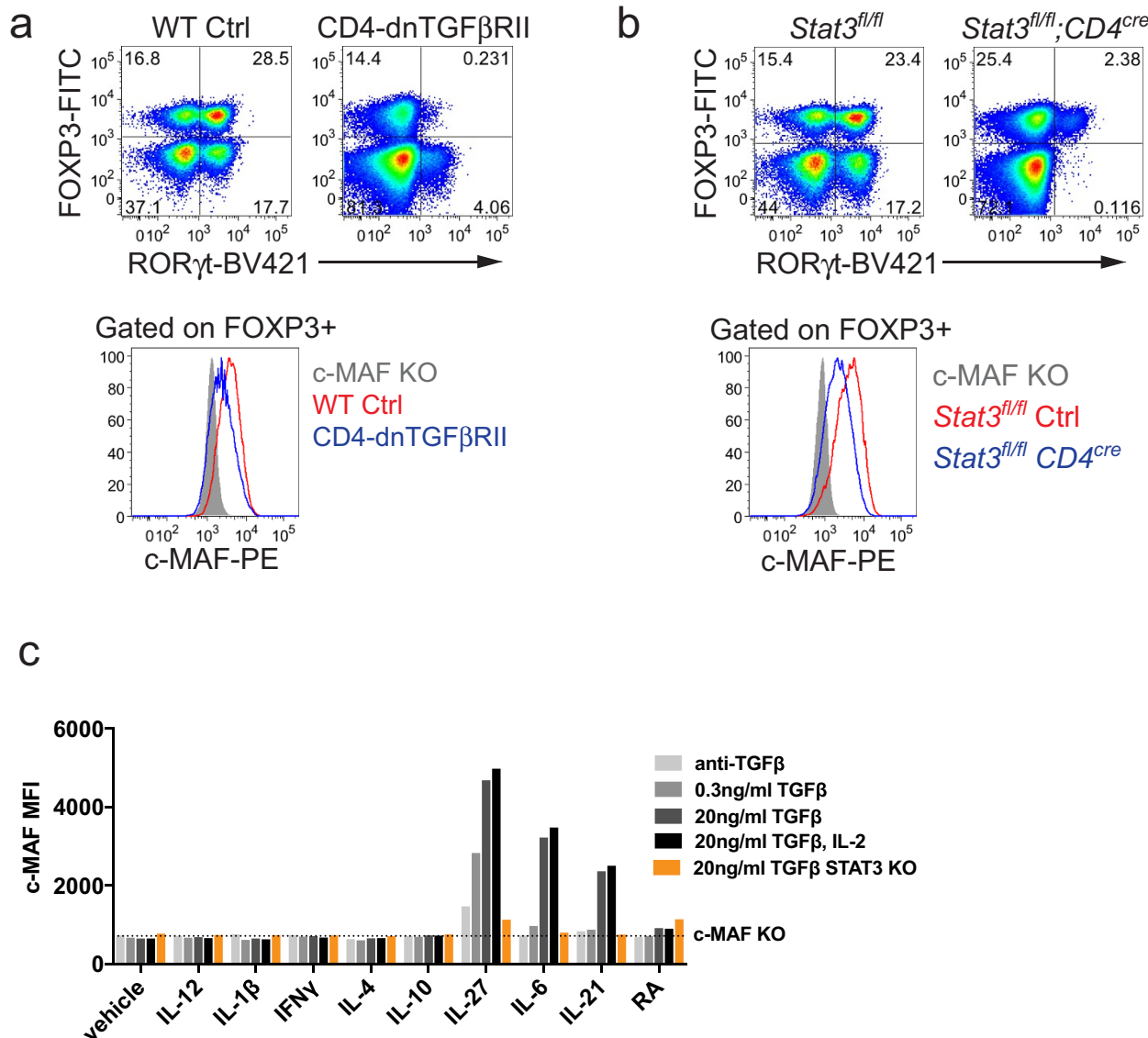
T cell reconstitution system. Two replicates represent two independent experiments. **e**, Schematic of experimental design. **f**, Flow cytometry plots indicating the sorting gates from two independent experiments. **g**, Flow cytometry plots showing FOXP3 and ROR $\gamma$ t expression in sorted FOXP3-YFP<sup>+</sup> cells from two independent experiments. **h**, Gene set enrichment analysis performed on RNA-seq dataset of c-MAF-sufficient versus -deficient iT<sub>reg</sub> (FOXP3-YFP<sup>+</sup>) cells ( $n = 2$  independent experiments) with a gene set of 33 ROR $\gamma$ t-dependent transcripts identified previously<sup>11</sup>. **i**, Top, representative flow cytometry plot of c-MAF expression in T<sub>H</sub>17 cells (FOXP3<sup>−</sup>ROR $\gamma$ t<sup>+</sup>) from LILP of control (black) and *Maf*<sup>Δ/Δ</sup> (red) mice. The c-MAF negative population is defined by gating on FOXP3<sup>+</sup>ROR $\gamma$ t<sup>−</sup> T<sub>reg</sub> cells from *Maf*<sup>Δ/Δ</sup> mice (solid grey). Bottom, frequency of c-MAF expression in T<sub>H</sub>17 cells in control ( $n = 6$ ) and *Maf*<sup>Δ/Δ</sup> ( $n = 9$ ) mice from 3 independent experiments.



Extended Data Figure 8 | See next page for caption.

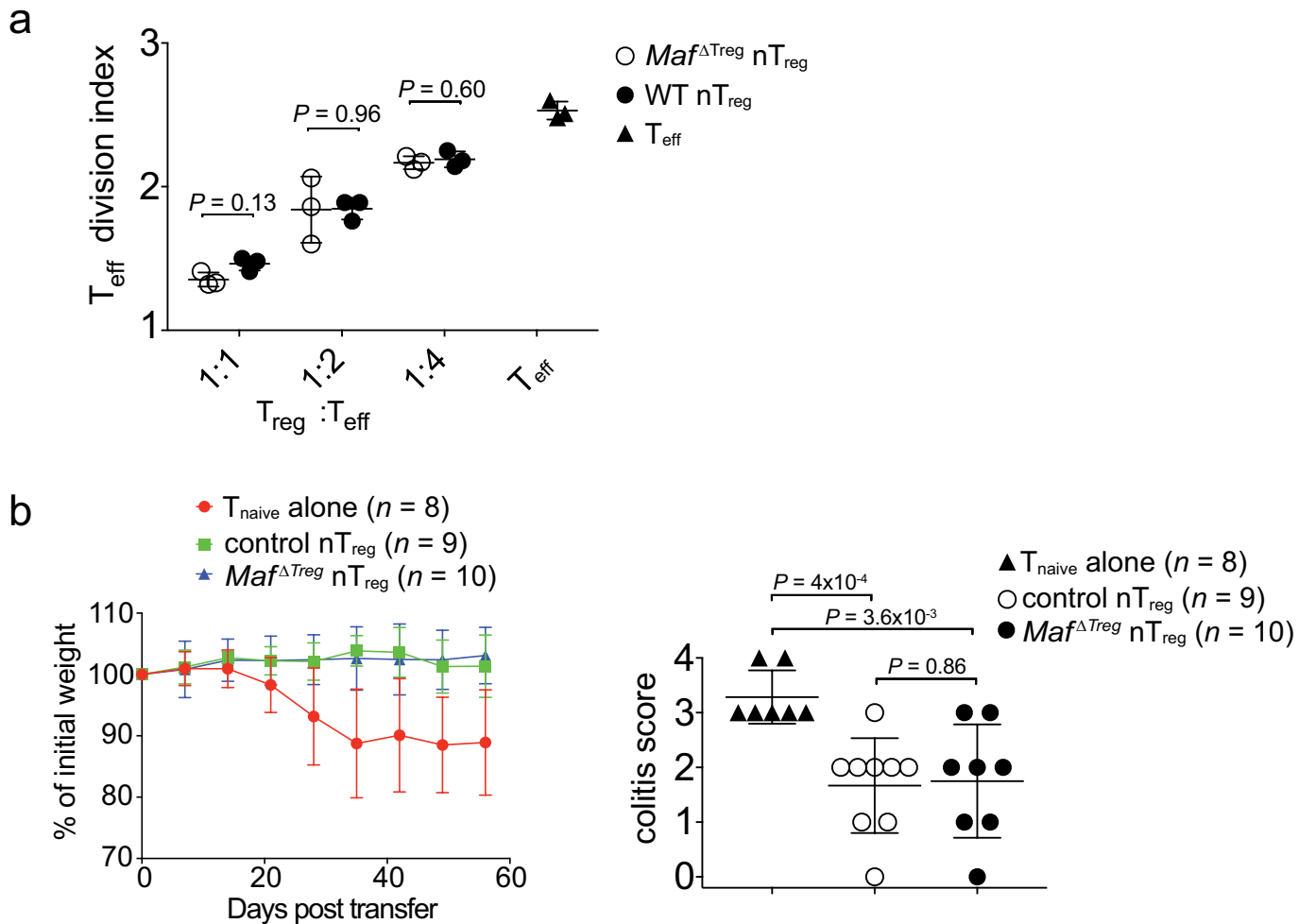
**Extended Data Figure 8 | Transcriptional profiling of conventional T<sub>H</sub>17 and *H. hepaticus*-specific T effector cells.** **a–f**, RNA-seq was performed on 2 biological replicates of each indicated condition. **a**, Flow cytometry analysis of HH7-2tg Teff cells from *H. hepaticus*-colonized mice and conventional IL-23R-GFP<sup>+</sup> (predominantly SFB-specific T<sub>H</sub>17) cells from SFB-colonized mice. GFP<sup>+</sup> gates in the bottom panel were used for sorting to perform RNA-seq. **b**, Principal component analysis of RNA-seq data from sorted cell populations. Coloured dots represent individual samples ( $n = 2$ ). **c, e, f**, Differentially expressed genes were calculated in DESeq2 using the Wald test with Benjamini–Hochberg correction to determine the FDR. Genes were considered differentially expressed when FDR < 0.1 and log<sub>2</sub> fold change > 1.5. **c**, Venn diagram depicting differentially expressed genes between indicated comparisons.

**d**, Significantly enriched disease pathways in the set of 149 shared genes upregulated in HH7-2tg *Maf*<sup>ΔTreg</sup> and HH7-2tg from anti-IL-10RA-treated mice compared to conventional large intestine T<sub>H</sub>17 cells. *P* values calculated by ingenuity pathway analysis using Fisher's exact test. **e**, Comparison of transcriptomes of *H. hepaticus*-specific T<sub>H</sub>17 cells from mice treated with IL-10RA blockade or *Maf*<sup>ΔTreg</sup> and conventional T<sub>H</sub>17 cells. Scatter plot depicting log<sub>2</sub> fold change of gene expression. Blue, red and purple dots indicate significant differences. **f**, Heat map depicting the 347 shared genes differentially expressed between pathogenic HH7-2 and conventional T<sub>H</sub>17 cells (purple dots in **e**). Data for each condition are the mean of 2 biological replicates. Scale bar represents *z*-scored variance stabilized data (VSD) counts.



**Extended Data Figure 9 | STAT3 and TGF $\beta$  signal synergistically to promote c-MAF expression.** **a**, Top, representative flow cytometry plots depicting ROR $\gamma$ t and FOXP3 expression in CD4 $^+$  T cells in the LILP of mice with a dominant-negative mutant of TGF $\beta$  receptors (CD4-dnTGF $\beta$ RII) and littermate controls ( $n = 3$ ). Bottom, representative plot of c-MAF expression in FOXP3 $^+$  cells from the indicated mice in the top panel. **b**, Top, representative flow cytometry plots depicting ROR $\gamma$ t and FOXP3 expression in CD4 $^+$  T cells in the LILP of Stat3 $^{fl/fl};CD4^{cre}$  and

Stat3 $^{fl/fl}$  littermate controls ( $n = 4$ ). Bottom, representative plot of c-MAF staining in FOXP3 $^+$  cells from indicated mice in the top panel. **c**, Mean fluorescence intensity of c-MAF staining in *in vitro* differentiated CD4 $^+$  T cells. Naive CD4 $^+$  T cells from wild-type, Stat3 $^{fl/fl};CD4^{cre}$  and *Maf* $^{fl/fl};CD4^{cre}$  mice were activated for 48 h with anti-CD3 $\varepsilon$ /anti-CD28 antibodies under indicated conditions. Dashed line represents the MFI of c-MAF in *Maf* $^{fl/fl};CD4^{cre}$  T cells. Data are from one of two independent experiments.



adoptively transferred with naive T cells alone ( $n=8$ ), or naive T cells in combination with nT<sub>reg</sub> cells from Maf<sup>ΔTreg</sup> ( $n=10$ ) or littermate control *Foxp3*<sup>creYFP</sup> ( $n=9$ ) mice. Data are a summary of two independent experiments. All statistics were calculated by unpaired two-sided Welch's *t*-test. Error bars denote mean  $\pm$  s.d. *P* values are indicated on the figure.

## Life Sciences Reporting Summary

Corresponding author(s): Dan R Littman

 Initial submission    Revised version    Final submission

Nature Research wishes to improve the reproducibility of the work that we publish. This form is intended for publication with all accepted life science papers and provides structure for consistency and transparency in reporting. Every life science submission will use this form; some list items might not apply to an individual manuscript, but all fields must be completed for clarity.

For further information on the points included in this form, see [Reporting Life Sciences Research](#). For further information on Nature Research policies, including our [data availability policy](#), see [Authors & Referees](#) and the [Editorial Policy Checklist](#).

## ► Experimental design

### 1. Sample size

Describe how sample size was determined.

Animal sample size estimates were determined using power analysis (power=90% and alpha=0.05) based on the mean and standard deviation from our previous studies and/or pilot studies using 4-5 animals per group.

### 2. Data exclusions

Describe any data exclusions.

No samples were excluded from analysis.

### 3. Replication

Describe whether the experimental findings were reliably reproduced.

All attempts at replication were successful.

### 4. Randomization

Describe how samples/organisms/participants were allocated into experimental groups.

For T cell adoptive transfer colitis co-housed littermate recipients were randomly assigned to different treatment groups such that each cage contained all treatment conditions.

### 5. Blinding

Describe whether the investigators were blinded to group allocation during data collection and/or analysis.

Pathology analysis was single-blind. All other animal studies were not blinded

Note: all studies involving animals and/or human research participants must disclose whether blinding and randomization were used.

### 6. Statistical parameters

For all figures and tables that use statistical methods, confirm that the following items are present in relevant figure legends (or in the Methods section if additional space is needed).

n/a Confirmed

- The exact sample size (n) for each experimental group/condition, given as a discrete number and unit of measurement (animals, litters, cultures, etc.)
- A description of how samples were collected, noting whether measurements were taken from distinct samples or whether the same sample was measured repeatedly
- A statement indicating how many times each experiment was replicated
- The statistical test(s) used and whether they are one- or two-sided (note: only common tests should be described solely by name; more complex techniques should be described in the Methods section)
- A description of any assumptions or corrections, such as an adjustment for multiple comparisons
- The test results (e.g. P values) given as exact values whenever possible and with confidence intervals noted
- A clear description of statistics including central tendency (e.g. median, mean) and variation (e.g. standard deviation, interquartile range)
- Clearly defined error bars

See the web collection on [statistics for biologists](#) for further resources and guidance.

## ► Software

Policy information about [availability of computer code](#)

### 7. Software

Describe the software used to analyze the data in this study.

Flow jo (v9.9.6,Tree Star) was used for all flow cytometry analysis. Prism7 (v7.0) was used to generate all graphs and statistics with the exception of RNA-seq. RNA-seq analysis was performed using STAR (v2.5.2b), featureCounts is part of the Subread package(v1.5.1), DESeq2 (v1.14.1), R (v3.3.1), ComBat is part of the sva R package (v3.22.0), Ingenuity Pathway Analysis ([www.ingenuity.com](http://www.ingenuity.com)). Gene set enrichment analysis (GSEA, <http://www.broad.mit.edu/gsea/>). Nucleotide sequences of the TCR $\alpha$  and TCR $\beta$  families were retrieved from the IMGT database (<http://www.imgt.org>). The potential MHCII epitopes were predicted with online software RANKPEP (<http://imed.med.ucm.es/Tools/rankpep.html>).

For manuscripts utilizing custom algorithms or software that are central to the paper but not yet described in the published literature, software must be made available to editors and reviewers upon request. We strongly encourage code deposition in a community repository (e.g. GitHub). *Nature Methods* [guidance for providing algorithms and software for publication](#) provides further information on this topic.

## ► Materials and reagents

Policy information about [availability of materials](#)

### 8. Materials availability

Indicate whether there are restrictions on availability of unique materials or if these materials are only available for distribution by a for-profit company.

No restricted materials were used. (Tetramers are available through the NIH tetramer core facility. TCRtg mouse lines have been deposited and will be available at Jackson laboratory)

## 9. Antibodies

Describe the antibodies used and how they were validated for use in the system under study (i.e. assay and species).

The antibodies are described below. All antibodies were purchased from BD, eBioscience, Biolegend or BioXcell. All antibodies were validated by manufacturers and in previous publications.

Antibodies for flow cytometry:  
 antibody/clone/color/company  
 CD3 145-2C11 AF700/PerCP-Cy5.5 BD  
 CD4 RM4-5 BUV395/PE-Cy7 BD  
 CD25 PC61 APC ebioscience  
 CD44 IM7 AF700 ebioscience  
 CD45.1 A20 BV421 BD  
 CD45.1 A20 APC-eF780/PerCP-Cy5.5 ebioscience  
 CD45.2 104 PerCP-Cy5.5/APC ebioscience  
 CD62L MEL-14 PE ebioscience  
 CXCR5 L138D7 PE Biolegend  
 NPR-1(CD304) 3E12 BV421 Biolegend  
 ST2 RMST2-2 PE ebio  
 TCR $\beta$  H57-597 APC-eF780/BV711 BD  
 TCR V $\beta$ 6 RR4-7 APC ebioscience  
 TCR V $\beta$ 6 RR4-7 FITC BD  
 TCR V $\beta$ 8.1/8.2 MR5-2 FITC BD  
 TCR V $\beta$ 14 14-2 FITC BD  
 Bcl-6 K112-91 BV421 BD  
 c-Maf T54-853 PE BD  
 Foxp3 FJK-16s FITC/PE-Cy7/APC ebioscience  
 GATA3 TWAJ FITC ebioscience  
 Helios 22F6 PE ebioscience  
 RORyt B2D APC/PE ebioscience  
 RORyt Q31-378 BV421 BD  
 T-bet eBio4B10 PE/APC ebioscience  
 IL-10 JES5-16E3 BV421 BD  
 IL-17A eBio17B7 APC ebioscience  
 IFN- $\gamma$  XM61.2 FITC Biolegend

Antibodies for cell culture and mouse treatment  
 antibody/clone/company  
 anti-CD3e 145-2C11 Bioxcell  
 anti-CD28 37.51 Bioxcell  
 anti-IL4 11B11 Bioxcell  
 anti-IFNg XMG1.2 Bioxcell  
 anti-TGF $\beta$  1D11.16.8 Bioxcell  
 anti-IL10Ra 1B1.3A Bioxcell

## 10. Eukaryotic cell lines

a. State the source of each eukaryotic cell line used.

The NFAT-GFP 58 $\alpha$ - $\beta$ - hybridoma cell line was kindly provided by Dr. K. Murphy.

b. Describe the method of cell line authentication used.

The NFAT-GFP 58 $\alpha$ - $\beta$ - hybridoma cell line can faithfully report TCR stimulation as shown in previous publications:

Yang et. al., Nature, 2014, 510(7503):152-6.

Ise et. al., Nat Immunol, 2010, 11(2): 129-135.

c. Report whether the cell lines were tested for mycoplasma contamination.

mycoplasma contamination was not tested

d. If any of the cell lines used are listed in the database of commonly misidentified cell lines maintained by [ICLAC](#), provide a scientific rationale for their use.

No commonly misidentified cell lines were used.

## ► Animals and human research participants

Policy information about [studies involving animals](#); when reporting animal research, follow the [ARRIVE guidelines](#)

### 11. Description of research animals

Provide details on animals and/or animal-derived materials used in the study.

WT C57Bl/6 mice were obtained from Jackson Laboratories or Taconic Farm. Il10<sup>-/-</sup>, CD4-dnTGFbRII, CD4cre, CD45.1, Foxp3creYFP, Il23rgfp, Maf fl/fl; Stat3 fl/fl and Gata3 fl/fl mice were on C57Bl/6 background. Littermates with matched sex (both males and females) were used. Except the aged mice (6-12 month old) analyzed in the experiments of Fig. 4e, mice in all the experiments were 6-12 week old at the starting point of treatments.

Policy information about [studies involving human research participants](#)

### 12. Description of human research participants

Describe the covariate-relevant population characteristics of the human research participants.

This study did not involve human research participants.

## Flow Cytometry Reporting Summary

Form fields will expand as needed. Please do not leave fields blank.

### ► Data presentation

For all flow cytometry data, confirm that:

- 1. The axis labels state the marker and fluorochrome used (e.g. CD4-FITC).
- 2. The axis scales are clearly visible. Include numbers along axes only for bottom left plot of group (a 'group' is an analysis of identical markers).
- 3. All plots are contour plots with outliers or pseudocolor plots.
- 4. A numerical value for number of cells or percentage (with statistics) is provided.

### ► Methodological details

5. Describe the sample preparation.

The detailed information is provided in the manuscript methods section 'Isolation of lymphocytes' and 'T cell culture', 'MHCII tetramer production and staining'

Intestinal tissues were sequentially treated with PBS containing 1 mM DTT at room temperature for 10 min, and 5 mM EDTA at 37°C for 20 min to remove epithelial cells, and then minced and dissociated in RPMI containing collagenase (1 mg/ml collagenase II; Roche), DNase I (100 µg/ml; Sigma), dispase (0.05 U/ml; Worthington) and 10% FBS with constant stirring at 37°C for 45 min (SI) or 60 min (LI). Leukocytes were collected at the interface of a 40%/80% Percoll gradient (GE Healthcare).

The Peyer's patches and cecal patch were treated in a similar fashion except for the first step of removal of epithelial cells.

Lymph nodes and spleens were mechanically disrupted.

Fluorescence-activated cell sorting and magnetic-activated cell sorting were used to further isolate indicated cells populations.

6. Identify the instrument used for data collection.

LSRII or Ariall (BD Biosciences)

7. Describe the software used to collect and analyze the flow cytometry data.

Diva (BD Biosciences) and Flowjo 9.9.6 (Tree Star)

8. Describe the abundance of the relevant cell populations within post-sort fractions.

The purities of sorted T cells were more than 98%

9. Describe the gating strategy used.

Based on the pattern of FSC-A/SSC-A, cells in the lymphocyte gate were used for analysis of T cell subsets. Singlets were gated according to the pattern of SSC-H vs. SSC-W. Positive populations were determined by the specific antibodies, which were distinct from negative populations.

Tick this box to confirm that a figure exemplifying the gating strategy is provided in the Supplementary Information.

# CORRECTIONS & AMENDMENTS

---

---

## CORRECTION

<https://doi.org/10.1038/s41586-019-0922-z>

### **Author Correction: c-MAF-dependent regulatory T cells mediate immunological tolerance to a gut pathobiont**

Mo Xu, Maria Pokrovskii, Yi Ding, Ren Yi, Christy Au,  
Oliver J. Harrison, Carolina Galan, Yasmine Belkaid,  
Richard Bonneau & Dan R. Littman

Correction to: *Nature* <https://doi.org/10.1038/nature25500>,  
published online 07 February 2018.

In this Letter, the ‘Competing interests’ statement should have stated: ‘D.R.L. consults for and has equity in Vedanta Biosciences.’ The original Letter has not been corrected.